

# V+ 2 Technical Manual Series: Extravasation Dosimetry Module

January 2025



**Renaissance Code Development, LLC**

310 NW 5<sup>th</sup> St., Suite 203

Corvallis, Oregon 97330

(541) 286-4428

<https://www.rcdsoftware.com>

Preparer: \_\_\_\_\_

Reviewer: \_\_\_\_\_

Approver: \_\_\_\_\_

## ABSTRACT

VARSKIN+ is a U.S. Nuclear Regulatory Commission (NRC) computer code originally used by staff members and NRC licensees to calculate occupational dose to the skin resulting from exposure to radiation emitted from hot particles or other contamination on or near the skin. These assessments are required by Title 10 of the *Code of Federal Regulations* (10 CFR) 20.1201(c). The extravasation dosimetry module (ExtravDose) was added in early 2025 to allow estimation of spatial and temporal radiation dose to tissues in proximity to injection points following an extravasation event.

## Table of Contents

LIST OF FIGURES.....	iv
LIST OF TABLES.....	vii
1.0 INTRODUCTION.....	9
2.0 EXTRAVASATION DOSIMETRY MODULE.....	10
2.1. Extravasation in Nuclear Medicine.....	10
2.2. General Tissue Anatomy for Extravasation Dosimetry.....	11
2.3. Fluid Flow Model.....	12
2.3.1. Flow During Administration (Stage 1).....	13
2.3.2. Flow After Administration (Stage 2).....	18
2.3.3. Boundary Conditions.....	24
2.3.4. Time Step Controller.....	26
2.4. Activity Concentration Model.....	28
2.5. Dosimetry Model.....	30
2.5.1. Extravasation Dosimetry in the Literature.....	30
2.5.2. Threshold Doses for Tissue Reactions.....	31
2.5.3. Photon Dosimetry.....	32
2.5.4. Alpha Dosimetry.....	35
2.5.5. Electron Dosimetry.....	37
3.0 Key Parameters.....	40
3.1. Key Output Parameters.....	42
4.0 BENCHMARKING.....	44
4.1. Co-60 Dosimetry Confirmation.....	44
4.2. Pure Alpha Decay.....	48
4.3. Am-241 Alpha Decay.....	53
4.4. Co-60 Photons.....	55
4.5. Pure Beta Decay.....	59
4.6. F-18 Comparison to Extravasation Calculation in the Literature.....	63
5.0 REFERENCES.....	66

## LIST OF FIGURES

Figure 2-1	Modeling timeline with multiple stages and example parameters for vascular-lymphatic removal and elevation. ....	11
Figure 2-2	Left: Interstitial components include fine vasculature bathed in extracellular fluid. Right: Extravasation fluid displaces extracellular fluid, increases the interstitial matrix volume, and irradiates the basal layer of the epidermis and tissue components in the matrix. ....	12
Figure 2-3	Graphic demonstrating infiltration and confined flow. Thin vertical dimension is exaggerated. ....	13
Figure 2-4	Relative elevation head is based on user-specified angles for (left) polar angle $\theta$ for tissue lift direction and (right) azimuthal angle $\varphi$ for tissue lift magnitude. ....	23
Figure 2-5	Boundary condition treatment for vertical flow. ....	25
Figure 2-6	Boundary condition treatment lateral flow. ....	26
Figure 2-7	Time step controller algorithm for Stage 2. ....	28
Figure 2-8	Relative probability of distance $r$ occurring in random sampling of a computational cell that is both source and target. ....	34
Figure 2-9	Alpha particle range in tissue. ....	36
Figure 2-10	Scaled absorbed dose distribution for 1 MeV electrons in water. ....	39
Figure 4-1	Input parameters for an advanced scenario. ....	44
Figure 4-2	Results screen showing the subject seven outputs in the bottom panel. ....	45
Figure 4-3	Results report (.csv format) for accumulated dose at the end of the analysis. ....	46
Figure 4-4	Results report (.csv format) for absorbed dose rate in the last timestep of the analysis. ....	46
Figure 4-5	Results report for Dose to ROI in the last timestep revealing the average dose over all calculational cells. ....	47

Figure 4-6 Results report for accumulated dose in the last timestep revealing four cells in excess of the 1 Gy dose threshold..... 48

Figure 4-7 Basic model inputs for a Gd-148 simulation..... 49

Figure 4-8 Accumulated Dose at the end of analysis for Gd-148..... 50

Figure 4-9 Activity concentration at the first timestep..... 51

Figure 4-10 Absorbed dose report at the first simulation timestep indicating alpha dose to source cells and to adjacent cells..... 52

Figure 4-11 Accumulated dose report for the final timestep. 17% of the 800 values (136) are greater than the dose threshold of 2 Gy..... 52

Figure 4-12 Simulation input for Am-241 problem..... 53

Figure 4-13 Simulation output for Am-241 problem..... 54

Figure 4-14 Simulation output for Am-241 problem..... 55

Figure 4-15 Basic inputs for a Co-60 simulation. .... 56

Figure 4-16 Results for a Co-60 simulation showing accumulated dose..... 56

Figure 4-17 Showing the four central source cells with activity at the first time step..... 57

Figure 4-18 Results reported for absorbed dose rate in calculational cells at 0.02 minutes after extravasation. The source (right) and target (left) cells are highlighted. .... 58

Figure 4-19 Input window for Y-90 example..... 59

Figure 4-20 Results report for accumulated dose over all calculational cells..... 60

Figure 4-21 Activity concentration in the calculational cells at the first timestep. .... 61

Figure 4-22 Absorbed dose rate in the calculational cells at the first timestep..... 61

Figure 4-23 Absorbed dose rate in the first time step from activity in the four central cells..... 63

Figure 4-24 Input parameters for a basic calculation with <sup>18</sup>F. .... 64

Figure 4-25 Timeline inputs for a basic calculation with  $^{18}\text{F}$ . ..... 64

Figure 4-26 Dose results for  $^{18}\text{F}$  extravasation in local tissue. .... 65

**LIST OF TABLES**

Table 2-1. Parameters of state for extravasation flow in a computational grid ..... 19

Table 2-2. Assumed vascular-lymphatic removal of extravasated fluid from affected tissue to support future comparisons to clinical observations and data ..... 22

Table 2-3. Function coefficients ..... 34

Table 3-1. Key parameters for extravasation flow and dosimetry. .... 40

Table 3-2. Additional features for advanced extravasation flow ..... 41

## ACKNOWLEDGMENTS

This report documents the work performed by Renaissance Code Development, LLC (RCD) for the U.S. Nuclear Regulatory Commission (NRC) under Contract No31310022C0011. Staff at the Pacific Northwest National Laboratory authored initial versions of VARSKIN (US NRC 1987), with later versions amended at Colorado State University (US NRC 1992), the Center for Nuclear Waste Regulatory Analyses (US NRC 2006), and Oregon State University (US NRC 2011; US NRC 2014; US NRC 2018). RCD performed the activities described herein on behalf of the NRC Office of Nuclear Regulatory Research, Division of Systems Analysis. This report is a product of RCD and does not necessarily reflect the views or regulatory position of the NRC.

The authors are indebted to B. Allen, S. Bush-Goddard, R. Flora, V. Shaffer, J. Tomon, M. Saba, and S. Sherbini for their support during development and maintenance of many of the dosimetry models now appearing in VARSKIN+.



## 1.0 INTRODUCTION

Extravasation Dose (ed.) is a new module in VARSKIN+ (V+) 2 for calculating local tissue dose from radiopharmaceutical extravasation during medical administration (Benke et al. 2023). Extravasation occurs when a radiopharmaceutical intended for the bloodstream leaks into surrounding tissue. It is a temporary condition in which radioactive material within the patient irradiates tissues near the site of administration for longer periods of time than if extravasation did not occur.

The developed extravasation dosimetry module is a time-dependent, multi-dimensional, and multi-physics code that breaks the region into mesh/voxel volumes for analysis. It simulates the injection of a fluid with a defined activity concentration that is then transported throughout a region while accounting for mixing (i.e., concentration changes). With the transport of the concentrated fluid, a subsequent calculation of the spatial dependent dose rates and accumulated doses to tissue resulting from the fluid transport is determined. Models have been developed with the goal of focusing on ease of use for the end user in terms of the minimal number of required inputs while ensuring a reliable solution is obtained to help inform the decision-making process.

The fluid flow model is written generically to account for the various mechanisms and forces that impact the net flow spatially (e.g., diffusion, advection, gravity, etc.). With time-dependent numeric solutions comes limitations on the size of the time steps taken while “marching” toward the end of the problem. This control has been handled internally by the model to ensure appropriate time steps are taken for the rate of change of the physical processes occurring.

The dose model accounts for doses received from alpha particles, electrons, and photons. The model considers dose to source and target voxels in the modeled region of interest (ROI). Dose rates for each time step are calculated in addition to accumulated dose for the analysis time-period.

Users have two levels of input options depending on needs. Users can perform:

- quick approximations based on a minimal set of basic inputs (Basic mode) or
- in-depth assessments utilizing advanced modeling features with an expanded set of input parameters (Advanced mode).

## 2.0 EXTRAVASATION DOSIMETRY MODULE

This section briefly introduces extravasation with relevant tissue anatomy and presents models used for tracking the movement of radioactive extravasated fluid in tissue near the site of administration, approximating three-dimensional (3D) spatial distributions of radionuclide activity concentrations in tissue, and calculating local radiological dose to tissue from the extravasation. Key parameters are highlighted with remarks on input parameter selection and qualitative sensitivity.

### 2.1. Extravasation in Nuclear Medicine

In nuclear medicine, radiopharmaceuticals are administered for systemic uptake, widespread redistribution, and targeted concentration within the patient's body. To accomplish this, the radiopharmaceutical is frequently delivered into one of the veins of the patient with an intravenous (i.v.) line or pump. Other administration methods, such as injections, are also possible and may be preferred depending on the treatment and radiopharmaceutical type. An understanding of what constitutes extravasation (Aquino-Guerrero; 2022) frames the scope for extravasation modeling. Along these lines, extravasation during radiopharmaceutical administration can result in abnormally high local tissue doses near the site of administration.

Leakage of radioactive material into surrounding tissue is a primary consideration for extravasation modeling. When the radiopharmaceutical directly enters the bloodstream, it spends very little time near healthy tissues at the administration site, is quickly mixed with flowing blood, and redistributed throughout the body. During extravasation, however, radiopharmaceutical fluid leaks into nearby tissue and is not immediately redistributed. Over time, continued extravasation substantially increases the radioactivity in healthy tissue and is problematic because it elevates radiation absorbed dose to healthy tissue without a medical benefit. Healthy tissue in the immediate vicinity of the extravasation is referred to as the "affected area." The largest time integrated concentrations and accumulated local tissue doses are more important to dosimetry and response, compared to peripheral tissue locations that experience diminished activity concentrations during clearance.

Natural processes such as normal fluid exchange, uptake via microvasculature, and lymphatic clearance eventually remove the radiopharmaceutical from the affected area, but these processes can be perturbed by extravasation, especially when appreciable extravasated fluid volumes (e.g., more than 10 ml) are involved. Clinical mitigation, such as elevating the affected area and applying a warm compress, can increase clearance rates from the affected area and reduce local tissue dose. Modeling aspects in Figure 2-1 relate to extravasated fluid flow within tissue. Extravasated fluid represents radioactive fluid in tissue from extravasation. Administration represents when additional radiopharmaceutical is entering the patient's body.

To accommodate changes in clinical conditions during an extravasation event, Figure 2-1 illustrates a modeling timeline with provisions for mitigative measures. Elevation of the affected area and applying a warm compress to influence fluid migration and vascular-lymphatic removal are specifically highlighted. Although local tissue dose tends to be highest at locations near extravasation origination points, substantial extravasated fluid migration can result in a high local tissue dose at other locations. Extravasated fluid migration within the affected area is modeled according to flow relationships. Vascular uptake and lymphatic clearance are modeled by combined removal rate of extravasated fluid from the affected area. Different removal rates can be accommodated for various layers of tissue and general biological states, such as stasis, degraded removal, or normal removal from the affected area. Radioactive decay acts on the total activity in the affected area.

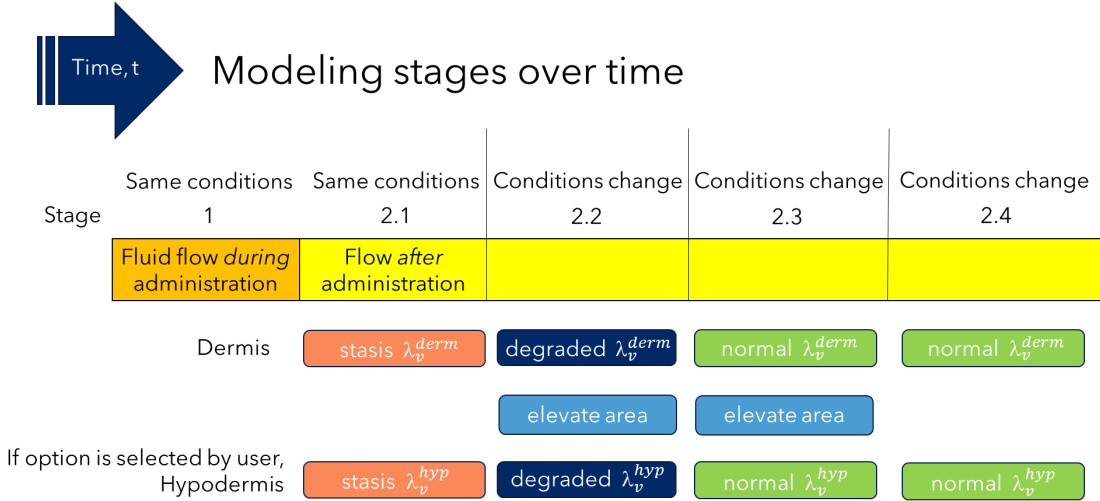


Figure 2-1 Modeling timeline with multiple stages and example parameters for vascular-lymphatic removal and elevation.

**2.2. General Tissue Anatomy for Extravasation Dosimetry**

Anatomical tissue representations are briefly discussed for the purposes of dosimetry. Many biochemical processes including ion transport that contribute to cellular, tissue, and organ function are beyond the scope of this work because primary mechanisms via individual or their collective ability to alter radiation dosimetry from extravasation have not been established. Because skin thickness and tissue composition vary at different locations on the body and among human populations, a multilayer model was constructed to accommodate a variety of potential extravasations, tissue locations, and patient specific characteristics. Either a different number of layers can be selected, or the calculation can proceed with a homogenous tissue matrix based on effective properties for the entire depth of tissue infiltrated during extravasation.

Figure 2-2 provides a simplified depiction of the interstitial matrix and fine vasculature with and without extravasation. In both cases, flow modeling based on homogeneous matrix properties may satisfactorily model bulk movements of extravasated fluid. Although extremely large infiltration rates combined with lower biological clearance rates can substantially, and temporarily, engorge tissue with extravasated fluid, subtle changes to the interstitial matrix are more likely when extravasation represents part of the administered fluid volume. For common intravenous administrations in the reticular dermis near the hypodermis, initial extravasation into the dermis and hypodermis are both credible depending on needle, catheter, or cannula placement and movement. When thickness and transmissive properties of the papillary dermis and reticular dermis are available, two dermal layers can be utilized.

By modeling extravasated fluid movement and concentration over time, local tissue dose within the affected area is calculated in three dimensions (3D). In humans, tissue water is approximately apportioned as  $\frac{2}{3}$  intracellular and  $\frac{1}{3}$  extracellular. Radionuclide-free water is expected to influence radiopharmaceutical dilution and in vivo dosimetry.



Figure 2-2 Left: Interstitial components include fine vasculature bathed in extracellular fluid. Right: Extravasation fluid displaces extracellular fluid, increases the interstitial matrix volume, and irradiates the basal layer of the epidermis and tissue components in the matrix.

To estimate potential stochastic and deterministic effects from extravasation, radiation absorbed doses are calculated to computational cell volumes in the tissue matrix.

### 2.3. Fluid Flow Model

The module supports two calculational modes: basic and advanced. A basic calculation is the default mode, and it applies simplifications for homogeneous tissue. Users invoke an advanced calculation with the Mode tab at the top of the main input screen.

As an input parameter for both basic and advanced calculations, the region width and length define the lateral extent of the tissue region of interest. These two dimensions apply physical limits for tracking the spread of radioactive fluid into distal tissue regions relatively far away from the site of extravasation. They have no influence on fluid flow or activity concentrations in tissue until radioactive fluid reaches one of the boundaries.

Timeline inputs are required and include the option for users to enter substages for clinical mitigative measures taken after the extravasation is discovered, such as applying a warm compress to the affected area and elevating the limb. Substages determine when particular aspects apply, such as different vascular-lymphatic removal rates induced by a warm compress or nonzero elevation head terms in flow equations due to elevation of the limb.

### 2.3.1. Flow During Administration (Stage 1)

When radiopharmaceutical extravasation occurs during administration, the volume of extravasated fluid increases over time. In this stage, extravasated fluid movement is modeled with an analytical solution based on a constant administration rate and effective parameters for the tissue matrix. Figure 2-3 illustrates the flow system. For the layered structure of this dermal system, “confined flow” means extravasation occurs in the matrix between impermeable layers above (e.g., epidermis) and below (e.g., fibrous connective tissue).

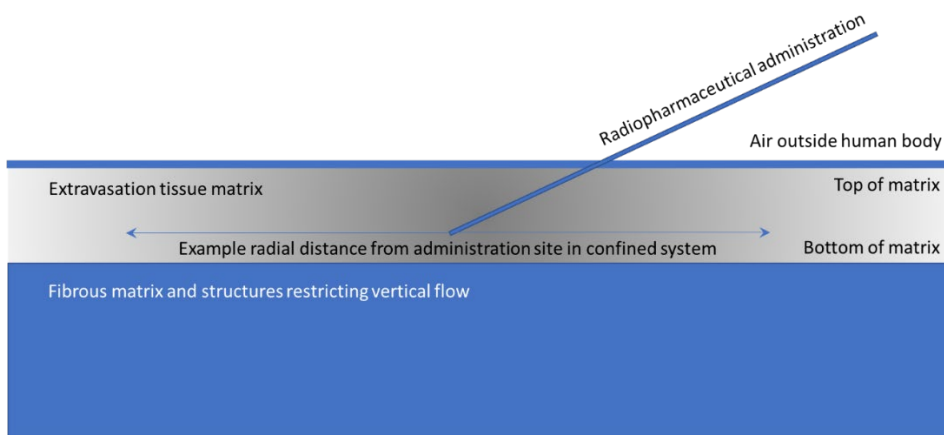


Figure 2-3 Graphic demonstrating infiltration and confined flow. Thin vertical dimension is exaggerated.

It is important to note that the source height in Figure 2-3 (e.g., tip of the radiopharmaceutical administration line) does not need to be specified in the current model because vertical mixing is rapidly achieved in this confined flow system within skin due to larger hydrostatic pressures induced from the continuous i.v. introduction of new extravasated fluid at the source location. During extravasation flow while the radiopharmaceutical is being administered, a restriction to vertical flow is anticipated due to underlying fibrous layers. Grey shading in the tissue matrix qualitatively depicts a hypothetical concentration gradient of extravasated fluid in tissue during forced administration flow. The spatial pressure gradient and resulting flow over time are calculated quantitatively.

The Theis equation (Masoodi and Ghanbari 2012) is utilized to calculate changes in the hydrostatic fluid pressure,  $p(r, t)$ , at various times and radial distances from the injection site (i.v. line) when fluid is pumped into the system. The analytical solution in Eq. [2.1] applies to a homogeneous representation for pressure-driven flow within a fibrous matrix or porous medium between confining layers:

$$p(r, t) = \frac{Q}{4\pi T} E_1 \left( \frac{S}{4T} \frac{r^2}{t} \right) \quad [2.1]$$

where

$Q$	Volumetric flow rate during extravasation [ $\text{ml h}^{-1}$ ]
$T$	Effective tissue transmissivity for extravasation lateral flow [ $\text{cm}^2 \text{h}^{-1}$ ]
$S$	Storage coefficient for extravasated fluid in tissue [unitless]
$r$	Radial distance from administration site [cm] and
$t$	Elapsed time for radiopharmaceutical extravasation during administration [h].

Units for hydrostatic pressure head are centimeters of water.

The Theis equation includes the exponential integral. Mathematical expressions for exponential integrals are briefly presented.

$$\text{In general form,} \quad E_n(z) = z^{n-1} \int_z^\infty \frac{e^{-x}}{x^n} dx \quad [2.2]$$

$$\text{For } n = 1, \quad E_1(z) = \int_z^\infty \frac{e^{-x}}{x} dx \quad [2.3]$$

The exponential integral is calculated for  $\left[ \frac{S}{4T} \frac{r^2}{t} \right]$ . Radial distance from the administration site is implemented with an array (size 100) of evenly spaced radial steps. Because the storage coefficient  $S$  is a relatively insensitive parameter for extravasation calculations, a unitless default value of 0.02 is used throughout. Eq. [2.1] yields a time-dependent hydrostatic pressure field.

Transmissivity is utilized in conjunction with a pressure differential. Because high Reynolds numbers for flow are not expected in the biological system, radial pressure differentials establishing the driving force for extravasated fluid flow are tracked according to the Darcy velocity,  $v$  [ $\text{cm h}^{-1}$ ], between two different radial positions from the site of administration:

$$v = -\left(\frac{T}{h}\right)\left(\frac{\Delta p}{\Delta r}\right) \quad [2.4]$$

where

$h$	Effective thickness of tissue for extravasation flow [cm]
$\Delta p$	Hydraulic pressure gradient [cm] and
$\Delta r$	Distance over which the pressure gradient applies [cm].

Evaluating Eq. [2.4] at many positions generates a radial velocity profile that is consistent with the pressure gradient from Eq. [2.1]. When the pressure gradient driving flow is established quickly relative to the duration of radiopharmaceutical administration, dynamic pressure effects at the very beginning of extravasation would not significantly alter time integrated activity concentrations or total local tissue dose from extravasation. Under these conditions, the time-dependence in Eq. [2.1] is simplified by assuming quasi-steady-state flow applies to the entire duration of extravasation. The bulk movement of extravasated fluid in tissue is calculated over time by applying this assumption to the Theis equation. Results from Eq. [2.1] coupled with the radial array are directly input as  $\frac{\Delta p}{\Delta r}$  into the calculation of fluid velocity in Eq. [2.4].

The velocity array calculated from Eq. [2.4] is used to solve for the travel time ( $\Delta t'$ ) of extravasated fluid flow between radial indices. The total travel time for an extravasated fluid packet from the administration site is represented by an elapsed time  $t$  which equals the summation of  $\Delta t'_i$  terms for the radial ring segments ( $r_i$ ) traversed. To implement and track these time-dependent relationships for quasi-steady-state flow, a polynomial regression is performed with the natural log of elapsed time,  $\ln(t)$ , and natural log of velocity,  $\ln(v)$ . The fitted velocity ( $v$ ) curve—constructed using coefficients from the polynomial fit and evenly spaced elapsed times—pairs elapsed times with fluid velocities for time step calculations of radial flow.

The radial position for an extravasated fluid packet based on its elapsed time is subjected to a power-law fit:

$$r_i = a(t_i)^b \quad [2.5]$$

with fitting coefficients  $a$  and  $b$ . According to the continuous extravasation (volumetric flow) rate and extravasation time inputs in Stage 1, mass balance and extravasated fluid flow are tracked with discrete extravasated fluid packets. Defining the extravasation of one fluid packet for a short time increment (e.g., 1 s) allows a large radial array of fluid positions to be generated.

The maximum radius for Stage-1 flow is determined by:

$$R = 1.1 \frac{Qt}{h} \quad [2.6]$$

where

$R$	Outer cylindrical model radius [cm]
$Q$	Extravasation volumetric flow rate [ $\text{ml h}^{-1}$ ]
$t$	Elapsed time for extravasation during radiopharmaceutical administration [h] and
$h$	Cylindrical tissue matrix height (sum of all tissue layer heights) [cm].

The factor of 1.1 in Eq. [2.6] ensures that the modeling domain for Stage-1 flow is slightly larger than the terms calculated in the fraction.

Extravasated fluid volume is calculated by gathering extravasated fluid packets in the same radial vicinity according to ten equally spaced radial rings. The 10<sup>th</sup> radial ring is set equal to the cylindrical radius,  $R$ . Ring spacing is one tenth of the cylindrical radius,  $\frac{R}{10}$ . Extravasated fluid volume in radial ring segment  $j$  is an input to Eq. [2.10]. It is calculated based on the number of extravasated fluid packets in that particular radial ring segment:

$$V_{r_j}(t) = \frac{\eta_{r_j}}{\eta} V_{ex}(t) \quad [2.7]$$

where

$V_{r_j}(t)$	Extravasated fluid volume in radial ring segment $j$ at time $t$ [ml]
$\eta_{r_j}$	Number of extravasated fluid packets in radial ring segment $j$ [-]
$V_{ex}(t)$	Radiopharmaceutical fluid volume extravasated at time $t$ , $Qt$ [ml]
$\eta$	Total number of fluid packets extravasated at time $t$ [-]

Diffusivity is not utilized during forced advective flows during time steps with radiopharmaceutical administration (Stage 1), but it is included in flow modeling after the administration ceases (Stage 2).

When similar transmissive properties apply to the entire thickness of tissue available for flow, transmissivity can be expressed as a product of effective parameters:

$$T = K h \quad [2.8]$$



where  $K$  represents the effective hydraulic conductivity for a homogeneous tissue matrix [ $\text{cm h}^{-1}$ ].

Equations [2.1], [2.4], and [2.8] pertain to flow within a homogeneous matrix. For extravasation in human tissue, Eq. [2.4] is intentionally written in terms of effective transmissivity and effective thickness. Additional relationships address extravasation in heterogeneous tissue. However, heterogeneous tissue is an optional selection that prompts the user to provide additional inputs, such as thicknesses and lateral transmissivities for each layer. However, heterogeneous tissue is an optional selection that prompts the user to provide additional inputs, such as thicknesses and lateral transmissivities for each layer. Despite its simplicity, homogeneous tissue modeling may be sufficient for many use cases when effective parameter inputs are representative of bulk transport and removal processes.

Because hydraulic conductivity is sensitive to the amount of fluid present, individual tissue layers or regions are not characterized by a singular value for hydraulic conductivity. Instead, transmissivities utilized by extravasation flow modeling account for the presence of additional fluid. As described by Eq. [2.8], transmissivity embodies the combined effects of hydraulic conductivity and thickness. Specifying additional parameters for heterogeneous tissue is optional but may provide more realistic modeling results when heterogeneities alter extravasation flow. When a heterogeneous tissue matrix is selected, the effective transmissivity for the tissue matrix is calculated as a weighted sum of transmissivity for individual layers:

$$T = \frac{\sum_{i=1}^m h_i T_i}{h} \quad [2.9]$$

where

$T$	Effective transmissivity for lateral flow in the tissue matrix [ $\text{cm}^2 \text{h}^{-1}$ ]
$h_i$	Effective thickness of the $i^{\text{th}}$ tissue for extravasation flow [cm]
$T_i$	Transmissivity for lateral flow in the $i^{\text{th}}$ layer of the tissue matrix [ $\text{cm}^2 \text{h}^{-1}$ ]
$i$	Index representing one of multiple layers [unitless] and
$m$	Total number of layers in the tissue matrix [unitless].

with  $h = \sum_{i=1}^m h_i$ . Unique parameters for tissue thickness and transmissivity can be assigned to each layer. These layer specifications affect flow calculations in Stage 1 and Stage 2. Time sequence results for extravasated fluid volumes infiltrating into tissue located at various radial positions in the confined flow system,  $V_{r_j}$  [ml], are distributed among multiple layers according to the ratio of transmissivity for the layer,  $T_i$ , to the transmissivity for all layers  $\sum_{i=1}^m T_i$ .

The extravasated fluid volume per unit tissue volume at various radial positions in each layer,  $\delta_{r_j,i}$  [ml cm<sup>-3</sup>], is calculated by dividing the infiltrating extravasated fluid volume,  $V_{r_j}$ , by the original tissue volume of that layer at radial position  $r_j$ . With an index  $j \in \{0,1, \dots, n\}$  for radial rings and index  $i \in \{1, \dots, m\}$  for layers within the tissue matrix, this calculation becomes

$$\delta_{r_j,i} = \left( \frac{V_{r_j}}{h_i A_{r_j}} \right) \left( \frac{T_i}{\sum_{i=1}^m T_i} \right) \quad [2.10]$$

where

$A_{r_j}$       Cross-sectional area for the  $j^{\text{th}}$  radial ring [cm<sup>2</sup>]

such that  $A_{r_j} = \pi r_j^2$  for radial ring  $j = 0$  from the central administration site to an outer radius,  $r_0$ , and  $A_{r_j} = \pi(r_j^2 - r_{j-1}^2)$  for radial rings  $j > 0$ .

Although start and end times for extravasation may not be well known in some situations, model time sequencing is based on user-specified inputs for the start and end times for extravasation. The radionuclide activity concentration of the radiopharmaceutical is based on the user-specified input.

As previously indicated, users are allowed to specify the width and length of the tissue region (e.g., tissue of the patient's arm closest to where extravasation occurs). The software recognizes if extravasated fluid is expected to reach the edge of the tissue region during forced administration flow in Stage 1. To avoid radioactive fluid flowing past the region boundary during Stage 1 for large volume extravasations, the software automatically increases the region dimensions. In Stage 2, radioactive fluid reaching a lateral boundary is allowed to exit the computational region. This flexibility allows users to devote computational resources to smaller tissue regions subjected to higher time-integrated activity concentrations instead of requiring calculations to be performed for the full dimensions of an extremity. Edge wrapping near the region boundary to follow the contours of human extremities is not presently modeled because the tissue geometry for flow modeling is assumed to remain flat. No vascular-lymphatic clearance of radioactive fluid is assumed to occur during the radiopharmaceutical administration.

### 2.3.2. Flow After Administration (Stage 2)

After forced flow conditions from radiopharmaceutical administration cease, 3D flow is modeled in lateral and vertical directions according to grid-based flow equations and sequential time steps. Changes in conditions, such as elevating the affected area, are implemented by updating input parameters in the appropriate time step. Because no

additional extravasated mass is added to the system after the radiopharmaceutical administration ceases, the total extravasated mass in the affected area decreases over time due radioactive decay, vascular-lymphatic removal, and flow outside the ROI.

Flow modeling after administration utilizes a 3D computational grid to calculate lateral and vertical extravasation flow within the affected area of tissue referred to as the ROI. Lateral flow occurs along tissue layers. Vertical flow occurs across tissue layers. Flow modeling equations are solved iteratively with a time step,  $\Delta t$ . Parameters of state are listed in Table 2-1. Hydrostatic pressure and the volume of extravasated fluid in each computational cell are recomputed for each time step. These parameters are utilized for lateral and vertical extravasation flow between two computational cells or between a computational cell on the perimeter across the boundary of the affected area. Elevation head differences are included for lateral flow between cells within a layer but not for vertical flow between overlying and underlying cells in the confined system.

Table 2-1 Parameters of state for extravasation flow in a computational grid

Symbol	Units	Parameter Description
$P_k$	cm	Hydrostatic pressure head at start of time step
$P'_k$	cm	Hydrostatic pressure head at end of time step
$V_k$	ml	Volume of extravasated fluid at start of time step
$V'_k$	ml	Volume of extravasated fluid at end of time step
$E_k$	cm	Elevation head relative to administration site

After administration ceases, transmissivity and diffusivity are utilized in conjunction with pressure and concentration gradients, respectively. For lateral flow within cubic computational grid, spatial dependency is modeled in Eq. [2.11] with a single lateral transmissivity relationship:

$$\Delta V_{k \leftarrow l} = \frac{\Delta t}{60} \left\{ T[(P_l + E_l) - (P_k + E_k)] \left( 1 \frac{\text{ml}}{\text{cm}^3} \right) + D \left( \frac{V_l - V_k}{s^2} \right) \right\} \quad [2.11]$$

where

- $\Delta V_{k \leftarrow l}$  Extravasated fluid volume flowing laterally into cell  $k$  from adjacent cell  $l$  during the time step [ml]
- $\Delta t$  Time step [min]
- $s$  Lateral distance between adjacent cells, side length for uniform cubic grid [cm]
- $P_k$  Hydrostatic pressure head in cell  $k$  [cm]

$P_l$	Hydrostatic pressure head in cell $l$ [cm]
$E_k$	Elevation head for cell $k$ relative to the site of administration [cm]
$E_l$	Elevation head for cell $l$ relative to the site of administration [cm]
$V_k$	Extravasated fluid volume in computational cell $k$ [ml]
$V_l$	Extravasated fluid volume in computational cell $l$ [ml]
$T$	Transmissivity for lateral extravasation flow within a tissue layer [ $\text{cm}^2 \text{h}^{-1}$ ] and
$D$	Diffusivity of extravasated fluid in tissue [ $\text{cm}^2 \text{h}^{-1}$ ].

For vertical flow within a cubic computational grid, the calculation is modified to account for half thicknesses of two vertically adjacent stacked tissue layers as well as the half thicknesses of extravasated fluid volumes in those layers to represent the distance over which the pressure gradient acts to induce flow. By accounting for the presence of extravasated fluid in the vertical distance between layers, vertical flow across the boundary takes the following form:

$$\Delta V_{k \leftarrow l} = \frac{\Delta t}{60} \left[ U \left( \frac{s}{d} \right) (P_l - P_k) \left( 1 \frac{\text{ml}}{\text{cm}^3} \right) + D \left( \frac{V_l - V_k}{d s} \right) \right] \quad [2.12]$$

where

$\Delta V_{k \leftarrow l}$	Extravasated fluid volume flowing vertically into cell $k$ from adjacent cell $l$ during the time step [ml]
$U$	Transmissivity of vertical flow across tissue layers [ $\text{cm}^2 \text{h}^{-1}$ ] and
$d$	Effective vertical distance between adjacent cells for flow modeling [cm].

such that the distance between stacked tissue layers, accounting for displacement of the extracellular fluid by the extravasated fluid with the same sized computational cells, reduces to

$$d = s + \left( \frac{V_k + V_l}{2s^2} \right) \left( 1 \frac{\text{cm}^3}{\text{ml}} \right) \quad [2.13]$$

where

$V_k$	Extravasated fluid volume for cell $k$ [ml]
$V_l$	Extravasated fluid volume for cell $l$ [ml] and
$s$	Vertical distance between adjacent cells, side length for uniform cubic grid [cm].

Fluid velocity is assumed to be small enough to neglect velocity head in the flow equations.

Positive  $\Delta V_{k \leftarrow l}$  results imply extravasated fluid flows into cell  $k$  from cell  $l$ . Negative  $\Delta V_{k \leftarrow l}$  results imply extravasated fluid flows from cell  $k$  into cell  $l$ . Constraints are applied to ensure volumes are not under- or over-filled by only transferring the amount fluid physically possible based on available cell volume and liquid volume to transport.

Vascular-lymphatic removal of extravasated fluid from the  $k^{\text{th}}$  computational cell at during each time step is determined as:

$$V_k^- = \frac{\lambda_v \Delta t}{60} V_k \quad [2.14]$$

where  $\lambda_v$  is the relative vascular-lymphatic removal rate [ $\text{h}^{-1}$ ]. If the user enters an absolute rate for vascular-lymphatic removal,  $\lambda_{v,abs}$  [ $\text{ml cm}^{-3} \text{h}^{-1}$ ], it is converted into a relative removal rate according to  $\lambda_v = \frac{\lambda_{v,abs} s^3}{V_k}$  for that time step.

The model assumes no vascular-lymphatic clearance during the period of administration and forced extravasation flow into affected tissue (Stage 1). In the current implementation of ExtravDose, basic and advanced calculations utilize a single vascular-lymphatic removal rate for the entire Stage-2 simulation time. The default value is  $0.15 \text{ h}^{-1}$ . If a warm compress event is included as a timeline input, a removal rate of  $0.25 \text{ h}^{-1}$  is used for that time period. To accommodate the availability of future data on clearance rates from various layers (e.g., dermis, hypodermis, or subcutaneous tissue), assumed example parameter values are provided in Table 2-2. The flow calculation is repeated until the maximum simulation time is reached or total extravasated fluid remaining in the affected area drops below a defined minimum volume.

Table 2-2 Assumed vascular-lymphatic removal of extravasated fluid from affected tissue to support future comparisons to clinical observations and data

Symbol	Parameter Description	Rates	Nominal Values
$\lambda_v^{derm}$	Vascular-lymphatic removal of extravasated fluid from dermis	Normal	0.12 h <sup>-1</sup>
		Degraded	0.03 h <sup>-1</sup>
		Stasis	0 h <sup>-1</sup>
$\lambda_v^{hyp}$	Vascular-lymphatic removal of extravasated fluid from hypodermis	Normal	0.18 h <sup>-1</sup>
		Degraded	0.08 h <sup>-1</sup>
		Stasis	0.02 h <sup>-1</sup>
$\lambda_v^{sub}$	Vascular-lymphatic removal of extravasated fluid from subcutaneous tissue	Normal	0.3 h <sup>-1</sup>
		Degraded	0.2 h <sup>-1</sup>
		Stasis	0.1 h <sup>-1</sup>
$\lambda_v^{homog}$	Vascular-lymphatic removal of extravasated fluid from homogeneous tissue	Normal	0.25 h <sup>-1</sup>
		Degraded	0.15 h <sup>-1</sup>
		Stasis	0.05 h <sup>-1</sup>

**Elevation Head.** When the affected area of tissue is elevated after extravasation to enhance lateral migration and clearance of extravasated fluid from the area, relative elevation head terms in Eq. [2.15] become nonzero. Tissue elevation is calculated relative to the site of administration (i.e., center of the affected area when extravasation occurs). In other words, the central computational cell is strictly assigned an elevation head of zero and located at the origin of the 3D grid. Relative elevation head at other computational cells equals the vertical component of their positions in 3D space relative to the origin. This vertical component depends on angles for tissue lift direction ( $\theta$ ) and tissue lift

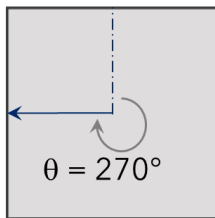
magnitude ( $\varphi$ ) shown in Figure 2-8 as well as the radial distance of the cell from the origin. Relative elevation head terms are active for user-specified start and end times for that tissue orientation and are calculated as in Eq. [2.15]:

$$E_k = r_k \cos(\theta - \theta_k) \sin(\varphi) \quad [2.15]$$

where

- $E_k$  Relative elevation head for the  $k^{\text{th}}$  computational cell [cm]
- $r_k$  Radial distance of the  $k^{\text{th}}$  computational cell [cm]
- $\theta_k$  Polar angle for the computation cell arranged within the grid [degrees]
- $\theta$  Angle for the lift direction [degrees] and
- $\varphi$  Tissue lift angle [degrees].

Polar angle determines direction



Azimuthal angle determines lift

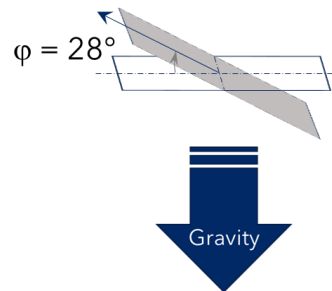


Figure 2-4 Relative elevation head is based on user-specified angles for (left) polar angle  $\theta$  for tissue lift direction and (right) azimuthal angle  $\varphi$  for tissue lift magnitude.

The general relationship above allows for multiple degrees of freedom in terms of lift direction and lift magnitude. However, a convenient simplification accommodates elevation of the entire limb (e.g., lifting an arm at the shoulder with a straight elbow or lifting a leg at the hip with a straight knee) by aligning the polar angle with the longitudinal direction of the limb. This simplification removes user specification for lift direction and provides elevation effects for a user-specified lift angle.

For implementing Eq. [2.11] for the flow of extravasated fluid after administration, lateral transmissivity is adjusted for the combined effects of hydraulic conductivity increases in fluid-filled tissue and potentially greater flow heights as follows:

$$T = T_0 \cdot x \left( \frac{V_k + V_l}{2 s^3} \right) \left( 1 \frac{\text{cm}^3}{\text{ml}} \right) \quad [2.16]$$

where

$T_0$	Nominal transmissivity of the tissue layer without extravasation [ $\text{cm}^2 \text{h}^{-1}$ ]
$V_k$	Extravasated fluid volume in cell $k$ [ml]
$V_l$	Extravasated fluid volume in cell $l$ [ml] and
$x$	Base of the power relationship [unitless default value of 2 is assumed].

As indicated by Eq. [2.16], lateral transmissivity is based on the amount of extravasated fluid present at that location. In this example, a unit volume of  $1 \text{ cm}^3$  is assumed for computational cells prior to extravasation. When extravasated fluid is present, transmissivity for Darcy flow is adjusted for each time step according to  $T(\bar{V}) = T_0 \cdot 2^{\bar{V}}$  with  $T_0$  representing nominal transmissivity of tissue without extravasated fluid present and  $\bar{V}$  representing the average extravasated volume for two adjacent computational cells between which extravasation flow is calculated.

Example spatial dependence of transmissivity based on extravasated fluid present: When  $T_0 = 2 \text{ cm}^2 \text{h}^{-1}$  represents transmissivity before extravasation and the power function base of 2 represents the influence of extravasated fluid on transmissivity, flow between computational cells with  $\bar{V}=0.5$  would be computed with  $T=2.8 \text{ cm}^2 \text{h}^{-1}$ . Flow in subregions with  $\bar{V}=1.2$  would be computed with  $T=4.6 \text{ cm}^2 \text{h}^{-1}$ . Due to a lack of biological data, initial values for the base of the power function (2) and nominal transmissivity ( $2 \text{ cm}^2 \text{h}^{-1}$ ) in this example are assumptions that can be updated as more data become available. Nominal lateral transmissivity is an advanced input parameter.

### 2.3.3. Boundary Conditions

Boundary conditions are defined such that extravasated fluid can flow outward of all exterior surfaces except from the top surface (positive-z direction; surface 0). The top surface is set as a hard/wall boundary allowing no fluid flow to cross to mimic the outer layer of skin. The other five boundaries create 'ghost cells' outside the exterior region with zero volume of extravasated fluid and utilizing the upstream pressure drop as an approximation to allow for a continuous pressure/flow profile. This mimics an infinite medium in the lateral directions and in the negative z-direction. It should be noted that extravasated fluid that leaves the region of interest is lost and cannot return back into the problem. If the user wishes to track the extravasated fluid beyond the boundary, the size of the region should be increased. The boundary conditions are handled and summarized for each lateral surface as shown in Figure 2-6.



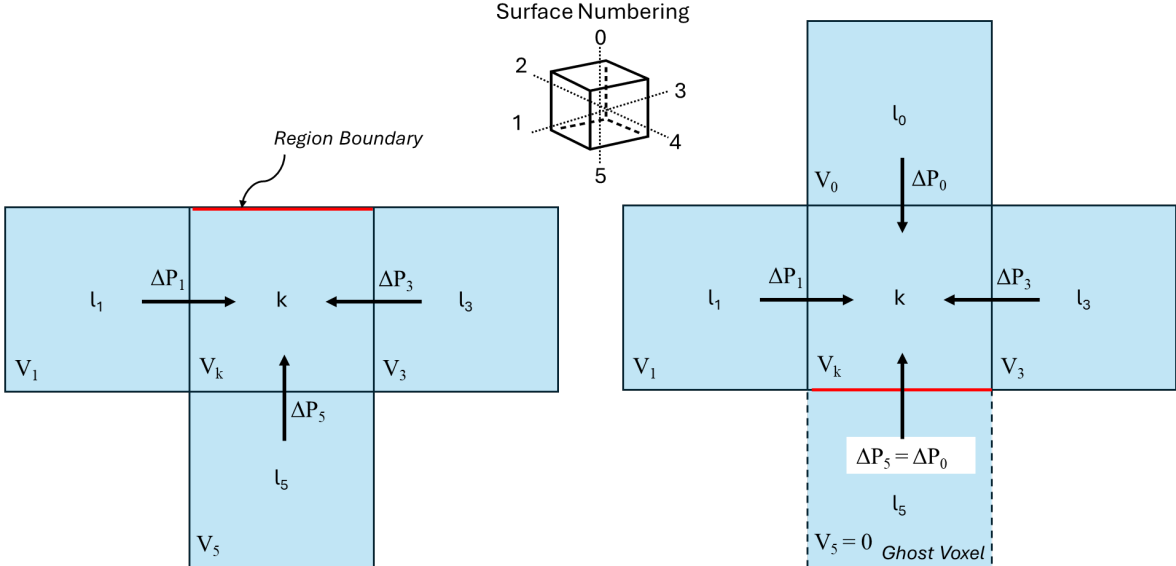


Figure 2-5 Boundary condition treatment for vertical flow.

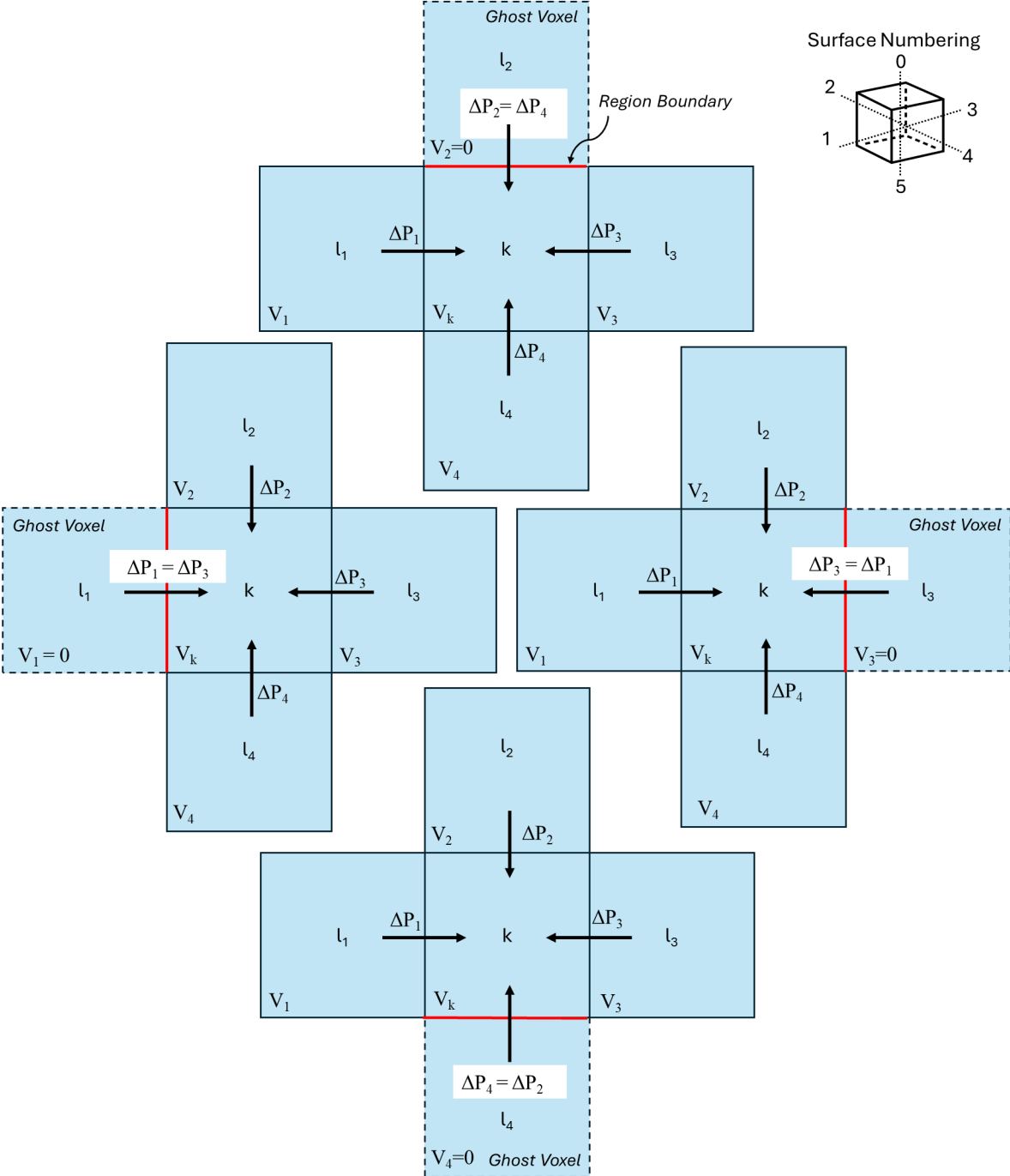


Figure 2-6 Boundary condition treatment lateral flow.

2.3.4. Time Step Controller

A time step controller is implemented to control the advancement of the explicit numeric scheme. Stage 1 calculations are performed at a constant 1 second interval. The first time-step size for Stage 2 is 0.5 seconds with a maximum allowed time step size ( $\Delta t_{max}$ )

of 5 seconds. After completion of a time step, the size of the next time step is determined following the logic of Figure 2-7. The first step determines the maximum time step size that satisfies the Courant number being less than or equal to 1.0, which is required because an explicit scheme is utilized:

$$C = \frac{\max|v| \cdot \Delta t_{Courant}}{\Delta x} \quad [2.17]$$

$$\Delta t_{Courant} = \frac{\Delta x}{\max|v|} \quad \text{with } C = 1.0$$

where

$C$	Courant number [-]
$v$	velocity across voxel surface [cm/min]
$\Delta t_{Courant}$	time step size [min]
$\Delta x$	voxel size [cm]

The max velocity across all voxel surfaces is based on the max volume transferred through a surface for a given time step with the use of Equation [2.20].

$$\max|v| = \frac{\max|\Delta V|}{\Delta x^2} \cdot \Delta t \quad [2.18]$$

where

$v$	velocity across voxel surface [cm/min]
$\Delta V$	volume transferred through voxel surface for a given time step [cm <sup>3</sup> ]
$\Delta t$	time step size [min]
$\Delta x$	voxel size [cm]

The minimum of the Courant time step and the previous utilized time step becomes the preliminary next time step size. Next, a limit on the rate of increase of the time step size is applied to ensure a stable solution is maintained. A third check for a buildup of oscillatory behavior reduces the timestep, as needed, to better resolve the time-domain and prevent further oscillations from growing. Oscillatory behavior is detected when an equal amount of fluid leaves and enters a voxel between two consecutive time steps. The last set of checks ensures that the minimum time step size ( $\Delta t_{\min} = 0.1$  seconds) and the maximum time step size ( $\Delta t_{\max} = 5.0$  seconds) are enforced.

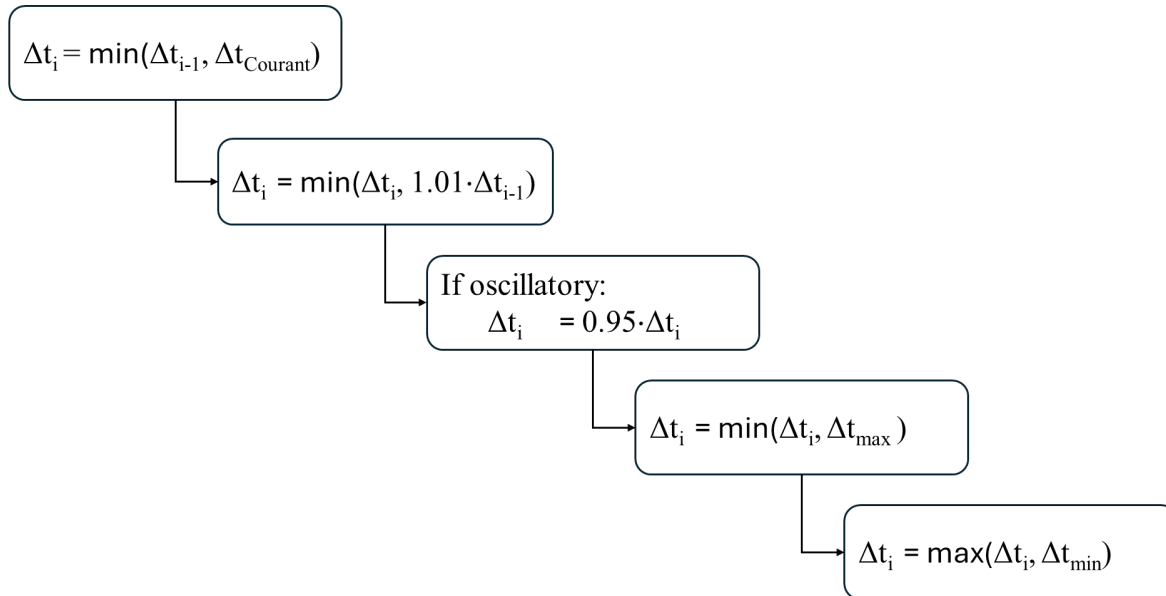


Figure 2-7 Time step controller algorithm for Stage 2.

## 2.4. Activity Concentration Model

The activity concentration model yields activity concentrations per unit tissue volume [Bq/cm<sup>3</sup>] in a regular computational grid for dosimetric calculations. Those calculations utilize a stationary 3D computational grid of tissue that does not flex or deform during extravasation and a uniform tissue density. These assumptions result in homogeneous stopping powers and linear attenuation coefficients throughout the tissue region for dosimetry.

Outputs of the activity concentration model adhere to the same assumptions and rely on two parameters:  $C$  and  $F$ . The parameter  $C$  represents the administered radiopharmaceutical activity concentration [Bq ml<sup>-1</sup>] and establishes the maximum activity concentration allowed in tissue [Bq cm<sup>-3</sup>]. In other words, activity concentrations in tissue cannot exceed the activity concentration of the administered radiopharmaceutical. The influence of mixing and dilution with nonradioactive fluid in tissue on subsequent dosimetric calculations is controlled by the fraction of nonradioactive fluid in tissue that is displaced by infiltrating extravasated fluid,  $F$  [unitless]. Displaced fluid is not available for mixing and dilution within the computational cell. Presently, a single value for  $F$  is applied to the entire region of interest (ROI).

The current implementation of ExtravDose calculates the activity concentration for each time step using  $F = 0.33$  according to the following relationship:

$$C_{k,i}^*(t) = \begin{cases} F_{k,i}^* C e^{-\lambda_r t} & \text{if } F_{k,i}^* \leq F \\ \frac{1}{(1 + F_{k,i}^* - F)} F_{k,i}^* C e^{-\lambda_r t} & \text{if } F_{k,i}^* > F \end{cases} \quad [2.19]$$

where

$C_{k,i}^*(t)$	Activity concentration in tissue [Bq cm <sup>-3</sup> ] at time $t$ [min]
$C$	Activity of radiopharmaceutical per unit extravasated fluid volume [Bq ml <sup>-1</sup> ]
$F_{k,i}^*$	Extravasated fluid at the location expressed as a fraction of the computational cell volume [unitless], $F_{k,i}^* = \left(\frac{V_{k,i}}{s^3}\right) \left[\frac{ml}{cm^3}\right]$ where $1 \text{ cm}^3 = 1 \text{ ml}$
$V_{k,i}$	Extravasated fluid volume in a computational cell at the $k^{\text{th}}$ location in the $i^{\text{th}}$ layer, output from the extravasation flow model [ml]
$s$	Lateral distance between adjacent cells, side length for uniform cubic grid [cm]
$F$	Fraction of nonradioactive fluid in tissue that is displaced during extravasation, $0 \leq F \leq 1$ [unitless] and
$\lambda_r$	Radioactive decay constant, relative rate of removal [min <sup>-1</sup> ].

such that  $C_{k,i}^* \leq C$  where  $1 \text{ cm}^3 = 1 \text{ ml}$ .

Biological processes during extravasation do not concentrate radioactivity to levels greater than those in the original radiopharmaceutical. Therefore, the constraint of limiting radioactivity concentrations in tissue to those that are no greater than the concentration of radioactivity in the originally administered radiopharmaceutical prevents excessive overestimation of dose to tissue from a subset of more extreme flow cases with a large buildup of radioactive fluid near the site of extravasation.

Because  $F = 0.33$  approximates the amount of extracellular fluid in tissue that may be more readily displaced during extravasation,  $F$  is not one of the initial input parameters for Basic and Advanced calculations. Extravasated fluid displacement of nonradioactive fluid in tissue and retention of remaining nonradioactive fluid for dosimetry is controlled by  $F$ , which may differ among large- and small-volume extravasations. For this reason, future versions may allow users to specify  $F$  values.

Radioactive decay is included in the activity concentration model. It is assumed that the user enters an activity concentration for the radiopharmaceutical at the beginning of administration (i.e.,  $t = 0$ ). The calculation is repeated across the grid of tissue cells for individual time steps.

## 2.5. Dosimetry Model

The concentration model described in Section 2.4 quantifies radionuclide activity concentrations in tissue for numerous computational cells in a stationary regular cubic grid comprising the affected area of tissue. The dose model receives the time-dependent activity concentration for each grid position such that the total activity per cell is determined as:

$$A_{k,i}(t) = C_{k,i}^*(t) \cdot s^3 \quad [2.20]$$

Dose rate to a target cell from a nearby source cell is proportional to the activity concentration in the source cell. The total dose rate to a target cell includes contributions from all source cells. The calculation is repeated for all target cells. Likewise, radiation dose to a particular target cell is proportional to the time integrated activity concentration in a given source cell and all source cells.

Extravasation dosimetry is based on:

- (1) a homogeneous tissue ( $\rho = 1.1 \text{ g cm}^{-3}$ ) medium containing both source and target computational cells;
- (2) a 3D grid structure of cubic cells of dimension  $s$ ;
- (3) an overall affected tissue volume approximated as  $W \times L \times D$ , where  $W$  and  $L$  are the width and length of the affected tissue field, and  $D$  is the tissue depth infiltrated by extravasate; and
- (4) the activity concentration in tissue from the extravasation flow model as a function of time.

Doses are calculated for photon, alpha, and electron emissions originating in source cells and depositing energy in target cells.

### 2.5.1. Extravasation Dosimetry in the Literature

A body of work over four decades regarding dosimetry at a radiopharmaceutical extravasation site has been reviewed (Minsky et al. 1987; Shapiro et al. 1987; Castronovo et al. 1988; Breen and Driedger 1991; Williams et al. 2006; Bonta et al. 2011; Kawabe et al. 2013; Tsorxe and Hayes 2021 & 2023; Tylski et al. 2021; Maucherat et al. 2021; Osborne et al. 2021a; Osborne et al. 2021b; Wilson et al. 2022; Mazzara et al. 2022; Berry and Kendrick 2022; Iori et al. 2023) and is summarized here. In an extravasation event, dosimetry at the injection site is dependent on the physical and chemical characteristics of the radiopharmaceutical, the biological forces of the tissue surrounding

the administration location, the radioactivity extravasated, radiological emissions and their energy, radiological decay, the volume of affected tissue, and biophysical movement and dissipation of the extravasated fluid.

The modeling effort for dosimetry at this stage of development focuses on the determination of integrated energy emission and absorption, and the volume of tissue impacted by that radiological energy. Most authors considered homogeneous activity concentrations of extravasated fluid throughout the affected tissue with some form of biological loss (Tiwari et al. 2024; Barry and Kendrick 2022; Mazzara et al. 2022) or complete decay of the radionuclide at the injection site (Shapiro 1987; Castronovo et al. 1988). The major difference, however, in modeling radiation dose following extravasation is with the estimation or prediction of the affected tissue volume.

Justification for affected volume ranges from mere assumption (Castronovo et al. 1988; Osborne et al. 2021b; Tsorxe and Hayes 2021 & 2023; Wilson et al. 2022) to the size of an extravasated fluid bulge (Kawabe et al. 2013); equivalent infused fluid volumes or factors thereof (Shapiro 1987; Barry and Kendrick 2022); biological indication, e.g., skin erythema or wet desquamation (Breen and Driedger 1991 Williams et al. 2006); or imaging techniques (Arveschoug et al. 2020; Tylski et al. 2021; Maucherat et al. 2021; Iori et al. 2023). Affected volumes were also chosen depending on the radiation emitted, for example, spherical radii equal to the mean free path for photons (Bonta et al. 2011) or equal to the maximum range of electrons (Minsky et al. 1987). Some authors utilized dose coefficients originally determined for other purposes or employed various other software routines including Medical Internal Radiation Dose (MIRD) or Monte Carlo methods (Shapiro 1987; Tylski et al. 2021; Osborne et al. 2021a; Osborne et al. 2021b; Tsorxe and Hayes 2021; Maucherat et al. 2021; Iori et al. 2023).

To date, no method found in the literature has addressed temporal- and spatial-dependencies of activity concentration, coupled with radiological and biological removal, as well as radiation-specific energy absorption techniques for extravasation dosimetry.

### 2.5.2. Threshold Doses for Tissue Reactions

Deterministic thresholds are briefly summarized to provide a perspective on the radiation injury potential to patients who may experience the highest local tissue doses from extravasations. Lower thresholds for deterministic effects to skin from ionizing radiation generally range from 2 to 6 Gy for a variety of source characteristics, tissue depths, and irradiation areas. ICRP (2007; 2012; 2017) defines a tissue reaction as: "Injury in populations of cells, characterized by a threshold dose and an increase in the severity of the reaction as the dose is increased further. Tissue reactions were previously called deterministic effects. In some cases, tissue reactions are modifiable by post-irradiation procedures including health care and biological response modifiers." Consistent with this

definition, and for the purposes of this summary, a radiation injury to skin is considered to have occurred with the presence of an observable tissue reaction.

NCRP (2010) associates no observable reactions expected for a radiation dose to skin below 2 Gy and potential erythema or epilation reactions for a skin dose between 2 and 5 Gy. In its discussion on justification and optimization for the medical exposure of patients, ICRP (2019) emphasizes a correct administration with radioactivity primarily localized in the target of interest so that radioactivity in the rest of the body will be maintained “below levels that may be considered unacceptable in terms of adverse tissue reactions” and references its supporting guidance (ICRP 2001). ICRP (2001) lists a threshold dose of 2 Gy for skin erythema (dry desquamation) followed by higher threshold doses for more serious tissue reactions to skin. Their thresholds for skin pertain to an acute, not chronic, exposure.

For a single acute exposure, ICRP (2012) lists dose thresholds of approximately 3 to 6 Gy for skin reddening and attributes threshold doses of about 4 Gy for temporary epilation and 5 to 10 Gy for skin burns and more severe injuries. The U.S. Department of Health and Human Services (HHS 2023) considers 3.5 to 5 Gy as the dose threshold for the least severe skin injuries such as erythema and edema. The International Atomic Energy Agency (IAEA 2020) assigns ~3 Gy as the threshold for secondary erythema and temporary epilation for the medical management of radiation injuries. Likewise, the Centers for Disease Control and Prevention (CDC 2023) indicates a threshold dose to skin of about 2 Gy for radiation injury including reddening, edema, and dry desquamation. Above 15 Gy, CDC (2023) suggests injuries of blistering with moist desquamation and possible ulceration and necrosis.

### 2.5.3. Photon Dosimetry

A point kernel method is implemented for photon dosimetry. Activity of the source cell and the dose location of the target cell are both approximated by central kernels in the computational grid separated by distance  $r$ . Considering only uncollided photons (i.e., no scatter component) over relatively short distances in tissue subjected to the highest dose rates, the point kernel equation [2.21] estimates photon absorbed dose rate,  $\dot{D}_\gamma(r)$ , in units of Gy/s, as:

$$\dot{D}_\gamma(r) = k \frac{A Y E_0}{4\pi r^2} \left( \frac{\mu_{en}}{\rho} \right) e^{-\mu r} \quad [2.21]$$

where

$k$	unit conversion [ $1.6 \times 10^{-10} \text{ J g MeV}^{-1} \text{ kg}^{-1}$ ]
$A$	activity in the calculational cell [ $\text{nt s}^{-1}$ ]
$Y$	emission yield [ $\gamma \text{ nt}^{-1}$ ]



$E_0$	uncollided photon energy [MeV $\gamma^{-1}$ ]
$r$	point-kernel distance [cm]
$\frac{\mu_{en}}{\rho}$	mass energy absorption coefficient [cm <sup>2</sup> g <sup>-1</sup> ] and
$\mu$	linear attenuation coefficient [cm <sup>-1</sup> ].

When the point kernel approach is based on central points in source and target computational cells, it provides a straightforward and accurate approximation for absorbed dose rate averaged over the target cell volume from radioactive emissions distributed within the source cell volume for most pairs of source-target cells in the computational region of interest.

Because geometric factors are highly sensitive to the distance between source points and target points, deviations occur between the point-kernel approximation and 3D volumetric solutions when the source and target cells are very close to each other including when the source and target are collocated (i.e., self-irradiation). These differences can exceed 20% (dependent on paired distance and photon energy) when the source and target cells are either collocated or adjacent. The photon dose is very likely minimal compared to electron and potentially alpha dose to target cells within the confines of extravasate influence.

Shultis and Faw (2000) illustrate a numerical modeling approach with random sampling of source emission points and target receptor points with the distance between the two relating to  $r$  in Eq. [2.21]. The probability density function,  $p(r)$ , of these random point kernel distances is referred to as a point-pair distribution. Figure 2-8 presents a histogram for a point-pair distribution in a 1 cm<sup>3</sup> cube that is both source and target (self-irradiation). This distribution was developed by randomly choosing a source point and a target point within the cube and determining the distance between the two, repeating the process many times. Based on Figure 2-8, the point-kernel distance used for cells that are both source and target is assumed to be two-thirds of the user-input cell side length (i.e.,  $r = \frac{2}{3}s$ ).

When source and target are different cells, the distance between computational cells,  $r$ , with centroid 3D coordinates of  $(x_1, y_1, z_1)$  and  $(x_2, y_2, z_2)$ , is calculated using Eq. [2.22]:

$$r = \sqrt{(x_2 - x_1)^2 + (y_2 - y_1)^2 + (z_2 - z_1)^2} \quad [2.22]$$

An empirical relationship to estimate  $\mu/\rho$  (in units of cm<sup>2</sup>/g) for tissue as a function of incident photon energy (in units of MeV) was developed and is given below in Eq. [2.23], which is appropriate for photon energies between 0.001 and 10 MeV.

$$\frac{\mu}{\rho}(E) = \frac{a_0 + \sum_{i=1}^9 a_i \ln^i E}{1 + \sum_{i=1}^7 b_i \ln^i E} \quad [2.23]$$

A similar function was developed (Eq. [2.24]) to approximate the energy-dependent value of  $\mu_{en}/\rho$  for tissue, again appropriate for photon energies between 0.001 and 10 MeV;

$$\frac{\mu_{en}}{\rho}(E) = \frac{a_0 + \sum_{i=1}^7 a_i \ln^i E}{1 + \sum_{i=1}^8 b_i \ln^i E} \quad [2.24]$$

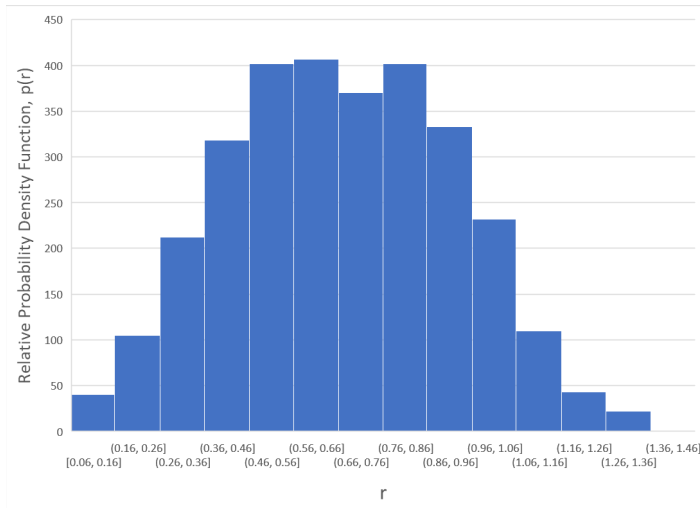


Figure 2-8 Relative probability of distance  $r$  occurring in random sampling of a computational cell that is both source and target.

Table 2-3 provides the coefficients for the fit of Eqs. [2.23] and [2.24] to the ICRU 44 (1989) data.

As the computational cell size becomes smaller, and without implementing point-pair distribution methods, calculation errors from utilizing Eq. [2.21] become small when determining the total local tissue dose received from radioactivity in numerous computational cells at short distances.

Table 2-3 Function coefficients.

Coefficient	Eq. [2.23]	Eq. [2.24]
a <sub>0</sub>	0.06997	0.03067
a <sub>1</sub>	-0.004154	0.01285
a <sub>2</sub>	-0.006919	-0.002061
a <sub>3</sub>	0.001211	-0.001057
a <sub>4</sub>	0.0005208	0.0003150
a <sub>5</sub>	-0.00005960	0.0001143
a <sub>6</sub>	-0.00002192	-0.00001012
a <sub>7</sub>	0.0000007728	-0.000005314
a <sub>8</sub>	0.0000007706	-
a <sub>9</sub>	-0.00000002494	-
b <sub>1</sub>	0.4296	0.5972
b <sub>2</sub>	0.03627	0.1361
b <sub>3</sub>	-0.005849	0.01239
b <sub>4</sub>	-0.000006259	-0.0006503
b <sub>5</sub>	0.0003312	-0.0003667
b <sub>6</sub>	0.00004527	-0.00005769
b <sub>7</sub>	0.000001844	-0.000004669
b <sub>8</sub>	-	-0.0000001555

#### 2.5.4. Alpha Dosimetry

Because alpha particles travel such short distances in tissue (i.e., on the order of tens of microns), a point kernel method for alpha dosimetry is not appropriate. Alpha dosimetry will follow a simple energy balance method where all emitted energy is apportioned to either the source cell or one of six immediately adjacent cells.

Generally, but depending on the dimensions of the calculational grid, a large fraction of alpha energy emitted in the source cell will be self-absorbed. Due to alpha emissions occurring very near the surfaces of the source cell, however, adjacent cells may also receive a small fraction of alpha energy. Assuming uniformly distributed alpha activity in the source calculational cell, the fraction of energy that could be lost to adjacent cells is equal to the volume of a thin cubical shell at the surface of the source cell divided by the volume of the total computational cell. The recoil atom is treated in the same fashion. In other words, those alpha particles (and the recoils) that originate very close to a surface of the cube are available to escape. The shell thickness is determined by the range of alpha particles based on their emission energy.

Alpha particle range in tissue ( $\rho = 1.1 \text{ g cm}^{-3}$ ) can be expressed as an empirical function [2.25] of initial alpha energy (in MeV):

$$R_{\alpha}[cm] = 8.382 \times 10^{-5} E^2 + 3.138 \times 10^{-4} E + 1.805 \times 10^{-4} \quad [2.25]$$

Resulting in the curve of Figure 2-9.

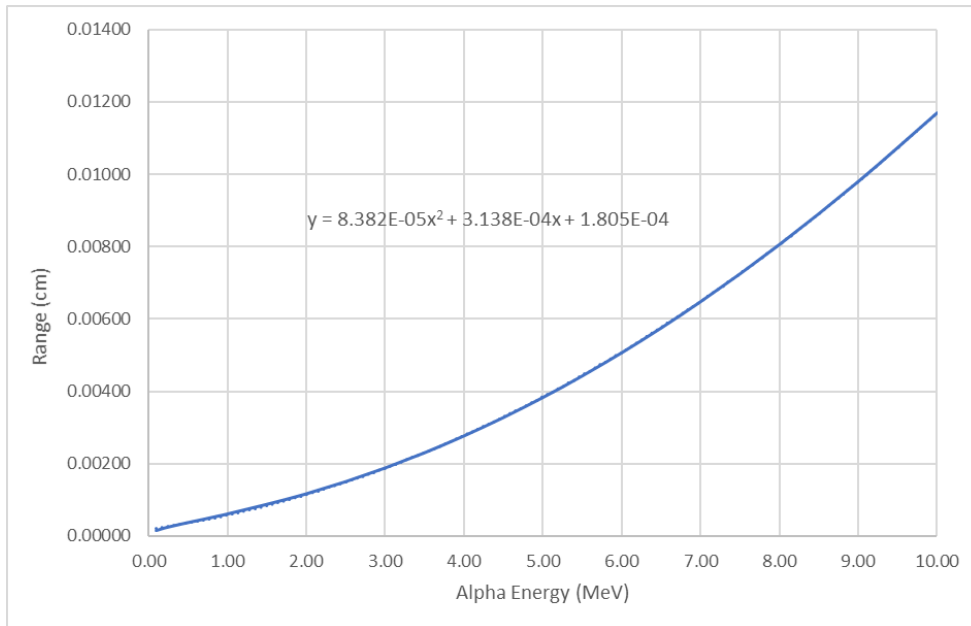


Figure 2-9 Alpha particle range in tissue.

As an example, it is first assumed that an alpha-emitting radionuclide is uniformly distributed in a 1 cm<sup>3</sup> source cell (a grid of 1 cm sides). If the emitted alpha particles possess an initial energy of 6 MeV, their travel distance in tissue is about 50 microns (0.005 cm). In this case, the volume of the shell in which alphas may escape the source cell is approximately

$$V_s = 6(1 \text{ cm})(1 \text{ cm})(0.005 \text{ cm}) = 0.030 \text{ cm}^3 \quad [2.26]$$

If half of the alpha energy originating in this shell is self-absorbed and the other half is conveyed outside the cell, the total fraction of alpha energy transported to adjacent cells can be approximated as

$$f = \frac{(0.5) 0.030[\text{cm}^3]}{1[\text{cm}^3]} = 0.015 \quad [2.27]$$

Assuming this energy is uniformly absorbed by each of 6 adjacent cells sharing a surface, the fractional energy absorption by an adjacent cell due to emissions in the source cell is

0.015/6 = 0.0025. This fraction is dependent on the source cell dimension,  $s$ , and the range (i.e., energy) of the alpha particle,  $R_\alpha$ .

Thus, the alpha absorbed dose rate (in units of Gy s<sup>-1</sup>) to the source cell can be shown (Eq. [2.28]) to equal

$$\dot{D}_{\alpha S} = k \frac{A Y E_{\alpha r}}{\rho s^3} \left(1 - 3R_\alpha/s\right) \quad [2.28]$$

while the absorbed dose rate to each of the six adjacent cells is (Eq. [2.29])

$$\dot{D}_{\alpha A} = k \frac{A Y E_{\alpha r}}{\rho s^3} \left(\frac{R_\alpha}{2s}\right) \quad [2.29]$$

In both equations, the parameters are:

$k$	unit conversion [1.6x10 <sup>-10</sup> J g MeV <sup>-1</sup> kg <sup>-1</sup> ]
$A$	activity in the computational cell [nt s <sup>-1</sup> ]
$Y$	emission yield [unitless]
$E_\alpha$	emitted alpha energy [MeV]
$E_{\alpha r}$	emitted alpha + recoil energy [MeV/nt]
$\rho$	tissue density [1.1 g cm <sup>-3</sup> ]
$s$	cell side length [cm] and
$R_\alpha$	alpha particle range for $E_\alpha$ [cm].

Because alpha particles have a very short range it is highly unlikely that multiple adjacent cells will be penetrated, even if the side length of a computational cell is reduced to 0.05 cm. Thus, for alpha dosimetry, it is assumed that only the source cell and those six target cells sharing a common surface will be impacted by source emissions. Once alpha energy deposition is summed over a given integration time, alpha dose is simply the sum of energy deposits divided by the mass of the computation cell.

### 2.5.5. Electron Dosimetry

Methods utilizing the SADCALC routine of SkinDose (Hamby et al. 2024) are employed for electron dosimetry. Electron dosimetry is fundamentally based on the point kernel concept such that electron absorbed dose rate,  $\dot{D}_e(r)$ , as a function of distance,  $r$ , is equal to

$$\dot{D}_e(r) = k \frac{A Y \overline{E}_e F_e(\xi, E_0)}{\rho 4\pi r^2 X_{90}} \quad [2.30]$$

where

$k$	unit conversion [ $1.6 \times 10^{-10} \text{ J g MeV}^{-1} \text{ kg}^{-1}$ ]
$A$	source activity in the computational cell [ $\text{nt s}^{-1}$ ]
$Y$	emission yield [ $\text{elec nt}^{-1}$ ]
$\overline{E}_e$	average electron energy [ $\text{MeV elec}^{-1}$ ];
$F_e(\xi, E_0)$	scaled absorbed dose distribution (SADD) [unitless]
$\xi$	scaling index for point kernel distance, ratio of $r$ to $X_{90}$ [unitless]
$\rho$	tissue density [ $1.1 \text{ g cm}^{-3}$ ]
$r$	distance between source and target [cm] and
$X_{90}$	distance from source in which 90% of electron energy is absorbed [cm].

The scaled absorbed dose distribution (SADD),  $F_e(\xi, E_0)$ , is similar to a relative Bragg curve as a function of initial electron energy,  $E_0$ . SADD values are central to the extravasation calculations.

The SADCALC routine in the SkinDose module was executed for every radionuclide available in the ICRP 38 and ICRP 107 (2008) database. From those calculations, values of  $X_{90}$ , the SADD distribution ( $F_e(\xi)$ ), average electron energy emitted ( $\overline{E}_e$ ), and electron emission yield ( $Y$ ) were all extracted to create a nuclide-dependent look-up table to estimate dose from a given source/target cell combination as a function of distance,  $r$ . As with photon dosimetry (Section 2.5.3), the point-kernel distance used for cells that are both source and target in electron dosimetry is assumed to be two-thirds of the user-input cell side length (i.e.,  $r = \frac{2}{3}s$ ).

In cases where the  $X_{90}$  of the selected nuclide is very short relative to the cubic side length,  $s$  (i.e.,  $X_{90} < s/4.5$ ), the electron energy emitted from a given source cell is assumed to be completely self-absorbed. The dose rate for this self-absorption is

$$\dot{D}_e = k \frac{A Y \overline{E}_e}{\rho s^3} \quad [2.31]$$

The fundamental SADD values are calculated for a unit-density, homogeneous water medium (Figure 2-10). Dose calculations in the Extravasation Dose module however assume a tissue density of  $1.1 \text{ g/cm}^3$ . This difference in density results in a slight shifting of the SADD distribution to the left (lower values of relative range), with a result assumed to be no greater than a few percent dependent on initial SADD value. This uncertainty is not expected to be any greater than the 10% difference introduced by using unit density for dose calculations.

**Example:** To calculate extravasation absorbed dose rate in tissue ( $\rho = 1.1 \text{ g/cm}^3$ ) at a distance of 0.1 cm from an electron source emitting monoenergetic electrons ( $\overline{E}_e = 1$

MeV/e<sup>-</sup>;  $X_{90} = 0.344$  cm) at a given activity ( $A = 10^9$  nt/s) and yield ( $Y = 1$  e<sup>-</sup>/nt), Eq. [2.30] is evaluated:

$$\dot{D}_e(r, E_0) = \frac{(1.6 \times 10^{-10})(10^9)(1) F_e(\xi, E_0)}{(1.1)(4\pi)(0.1)^2(0.344)} = 3.36 \cdot F_e(\xi, E_0) \quad [2.32]$$

As mentioned above, the SADCALC routine calculates the scaled absorbed dose distribution (SADD) for electrons as a function of energy  $E_0$  and relative to its  $X_{90}$  range. Figure 2-10 presents the SADD for 1 MeV electrons, as generated by SADCALC.

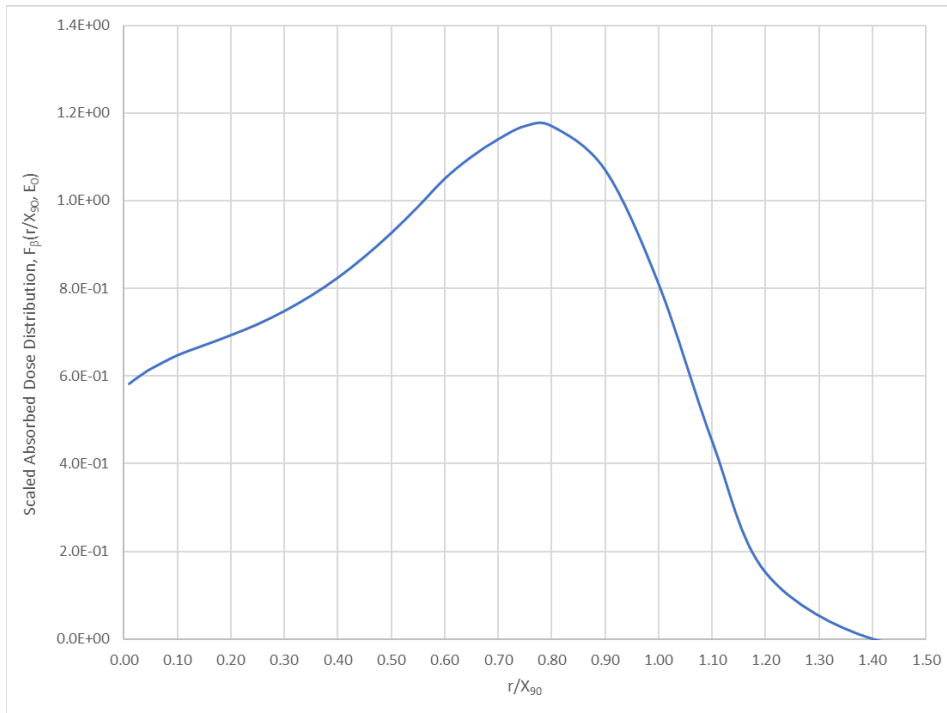


Figure 2-10 Scaled absorbed dose distribution for 1 MeV electrons in water.

In this example, the x-axis index ( $r/X_{90}$ ) is 0.291 (0.1/0.344) for a distance of 0.1 cm, and SADD ( $F_e(\xi)$ ) is 0.743 (unitless). Therefore, the point kernel electron dose rate at distance  $r$  is:

$$\dot{D}_e = 3.36 \cdot 0.743 = 2.5 \left[ \frac{\text{Gy}}{\text{s}} \right] \quad [2.33]$$

This result can be confirmed by V+ SkinDose. For a 1 MeV electron point-source, decay rate of 1 GBq, depth (distance) of 0.1 cm in material of density 1.1 g/cm<sup>3</sup>, an exposure time of 1 second, an averaging area of 0.001 cm<sup>2</sup>, and air backscatter correction disabled, SkinDose predicts the same electron dose rate of 2.5 [Sv/s].

### 3.0 Key Parameters

Key modeling parameters are described in Table 3-1 for basic extravasation calculations. In addition to the tissue heterogeneity and time-dependent inputs allowed in advanced calculations, Table 3-2 highlights two additional modeling parameters that automatically adjust lateral transmissivity based on the amount of extravasated fluid present.

Table 3-1 Key parameters for extravasation flow and dosimetry.

Param.	Remarks on Parameter Uncertainty and Input Selection
Q	Extravasation flow into tissue depends on (i) volumetric flow rate of the radiopharmaceutical during Stage 1 administration and (ii) radiopharmaceutical leakage into tissue. When radiopharmaceutical activity concentrations entering the patient vary significantly during administration (e.g., activity concentration or total extravasated activity differences of more than 50% within 10-min time intervals), users are encouraged to approximate extravasation with the largest fraction of extravasated fluid and longest extravasation consistent with clinical observations. Refinements to this approximation become more justified when the total dose to tissue is strongly influenced by Stage 1 activity concentrations in tissue. When time integrated activity concentrations dominate absorbed dose in the affected area, further refinements to modeling assumptions for the administration stage are not necessary.
$T$	Effective transmissivity of extravasated fluid in tissue is highly influential. Spatial dependency is addressed by a functional relationship acting on the amount of extravasated fluid infiltrating a computational cell (refer to Table 3-2).
$h$	Users enter the thickness of tissue receiving extravasated fluid. When no infiltrated thickness is known, 1.5 times the depth of the extravasation point can serve as an initial approximation for $h$ . Overestimating $h$ has the potential to result in lower activity concentrations in tissue. The option to supply inputs for multiple heterogeneous tissue layers allows thicker confined flow systems to be modeled within an infiltration tissue thickness of $h$ . This option can mitigate bulk volumetric dilution effects that can occur with homogeneous layer assumptions, because some heterogeneous layers can be highly restrictive to accepting and accommodating continuous flows of extravasated fluid.
$\lambda_v$	Although vascular-lymphatic removal is not modeled during Stage 1, it is expected to be influential in Stage 2. By utilizing substages in post-administration modeling, a transition of removal rates can be applied to



	capture salient effects (e.g., new removal rates for local circulation improvements from applying hot compresses to the area). Because overestimating $\lambda_v$ will underestimate extravasation dose to tissue, the smallest values of $\lambda_v$ supported by clinical observations are appropriate. This parameter is not available for user specification in the current ExtravDose implementation.
$U$	The flow model includes a separate parameter for vertical transmissivity, which can differ from that for lateral flow. Given the layered structure of tissue, biological cell networks, and interstitial spaces within skin, these structural effects can result in smaller vertical hydraulic conductivities and transmissivity compared to their lateral counterparts and suggest $U \leq T$ . Users can specify this parameter in an Advanced calculation.
$D$	Diffusivity of extravasated fluid in tissue is included in Stage-2 flow modeling and operates on concentration gradients. Transport from diffusion is calculated by the extravasation flow model. Diffusivity parameter values are typically more than an order of magnitude below transmissivity values. In other words, diffusion seldom dominates contaminant transport when advective flow also occurs. An initial default value of approximately $0.1 \text{ cm}^2 \text{ h}^{-1}$ (Aijaz et al., 2021; Grodzinsky 2011) is suggested until clinical extravasation data become available. Users can specify this parameter in an Advanced calculation.

Table 3-2 Additional features for advanced extravasation flow

Param.	Remarks on Parameter Uncertainty and Input Selection
$T_0$	$T_0$ represents nominal transmissivity without extravasated fluid present. $T_0$ can be expected to take values on the order of $1 \text{ cm}^2 \text{ h}^{-1}$ as loosely supported by biological analogs (Grodzinsky 2011), $T_0$ for extravasation cases is expected to exhibit a range over the patient population and would benefit from extravasation data collection efforts. For example, hydration status and other medical conditions of the patient can greatly influence hydraulic conductivity and $T_0$ (Aukland and Reed, 1993). As described for the power-base parameter $x$ , effective transmissivity can increase considerably (e.g., by an order of magnitude or more) due to appreciable extravasation. For these reasons, parameter values for $T_0$ and $x$ should be considered jointly and should be consistent with clinical observations. This parameter is not available for user specification in the current ExtravDose implementation.

$x$	The power base $x$ determines spatial variations in transmissivity for flow between two adjacent computational cells. Edema has been reported to increase hydraulic conductivity by a factor of more than 100,000 (Auckland and Reed, 1993; Guyton et al. 1966). Although extravasation increases may not include the upper-most range of edematous effects, provisions in the model allow for a variety of influences. In areas with large tissue bulges due to extravasation, effective transmissivity may increase to tens of $\text{cm}^2 \text{h}^{-1}$ temporarily. Parameter values for $T_0$ and $x$ should be considered jointly and should be consistent with clinical observations. This parameter is not available for user specification in the current ExtravDose implementation.
-----	---

The storage coefficient,  $S$ , in Eq. [2.1] is not included as an input parameter, because bulk flow exhibited limited sensitivity to this parameter for the time frames and radial distances of the greatest interest to extravasation dosimetry. A single value of approximately  $S = 0.02$  appears to be sufficient for a broad range of cases, because extravasated fluid velocities—calculated from the difference of two exponential integrals—become very insensitive to  $S$  for typical transmissivities and administration durations less than 2 h.

### 3.1. Key Output Parameters

In the lower portion of the Results window, the user will find seven additional output parameter values that may be of interest. Those parameters are defined below:

**Extravasated Volume.** The product of extravasation flow rate and extravasation duration. Extravasated volume indicates the total amount of fluid infiltrating tissue.

**Extravasated Activity.** The product of activity concentration for the radiopharmaceutical and extravasated volume. Extravasated activity indicates the total source activity for the calculation.

**Maximum Voxel Dose.** The maximum time-integrated absorbed dose in a given computational cell during the analysis period.

**Maximum Voxel Dose Rate.** The maximum absorbed dose rate in any computational cell over the entire user-specified region and analysis period.

**Time to Maximum Voxel Dose Rate.** The time from the beginning of extravasation to when the maximum voxel dose rate is reached.

**ROI (Region of Interest) Exceeding Threshold.** The percentage by volume of computational cells within the user-specified region that exceed the user's dose notification threshold.

**Dose to ROI.** The time-integrated absorbed dose, inclusive of all computational cells in the user-specified region of interest. Dose to region is an average dose to all tissue in the specified ROI.

## 4.0 BENCHMARKING

There are seven output parameters given to the user in the Results window. These parameters update dynamically while ed. is running, but then remain constant after the simulation is complete. The purpose of this section is to verify each of the outputs with a hand calculation as far as practicable. After the seven outputs are confirmed, the report goes into detail calculations for alpha, electron, and photon dosimetry by calculational cell.

### 4.1. Co-60 Dosimetry Confirmation

Cobalt-60 (ICRP 107) is chosen for the initial confirmation because it has a long half-life (5.27 yrs) and decays by beta transition (100% yield) resulting in the release of two gamma-ray photons (1.173 and 1.332 MeV) and a continuous spectrum of electrons (average of 0.0965 MeV). The electrons have an  $X_{90}$  range of 0.033 cm.

In the Advanced mode, using the default timeline (5-minute extravasation and 30-minute analysis), the inputs of Figure 4-1 were simulated.

The screenshot shows the 'V+ Extravasation Dosimetry v1.0' software interface. The window title is 'ed Extravasation Dosimetry v1.0'. The menu bar includes 'File', 'Mode', and 'Help'. The main title is 'V+ Extravasation Dosimetry v1.0' and 'MODEL INPUTS'. The RCD logo is in the top right corner.

**Source and Concentration Inputs**

- Database:  ICRP-38  ICRP-107
- Concentration: 500.000 MBq/mL
- Nuclide: Co-60
- Flow Rate: 0.200 mL/min

**Layer Inputs**

- Tissue Model:  Homogeneous  Heterogeneous
- Number of Layers: 1
- Layer 1:
  - Effective Tissue Thickness: 5.000 mm
  - Lateral Transmissivity: 0.010 cm<sup>2</sup>/h

**Transport Inputs**

- Dose Notification Threshold: 1.000 Gy
- Region Width: 10.000 cm
- Region Length: 10.000 cm
- Vertical Transmissivity: 1.000 cm<sup>2</sup>/h
- Fluid Diffusivity: 0.010 cm<sup>2</sup>/h
- Voxel Side Length: 5.000 mm

**Diagram**

The diagram shows a cross-section of skin layers with labels: Epidermis (~0.1 mm), Dermis (~1 mm), and Hypodermis (~1-5 mm). A note below the diagram says 'Not to scale'.

At the bottom of the interface are three buttons: 'Timeline', 'Calculate', and 'Results', along with a small RCD logo.

Figure 4-1 Input parameters for an advanced scenario.

The lateral transmissivity and fluid diffusivity inputs were both reduced to 0.01 cm<sup>2</sup>/h to slow the movement of material from the injection point and to inhibit radioactivity from spilling out of the Region of Interest (ROI) during the analysis period.

The first confirmation involves the two parameter outputs on the left side in the bottom panel of Figure 4-2. With inputs of activity concentration in the extravasated fluid of 500 MBq/mL and an extravasated volume of 1 mL, an Extravasated Activity of 500 MBq is confirmed. Likewise, with an input flow rate of 0.2 mL/min and an extravasation time of 5 minutes, an Extravasated Volume output of 1 mL is confirmed.

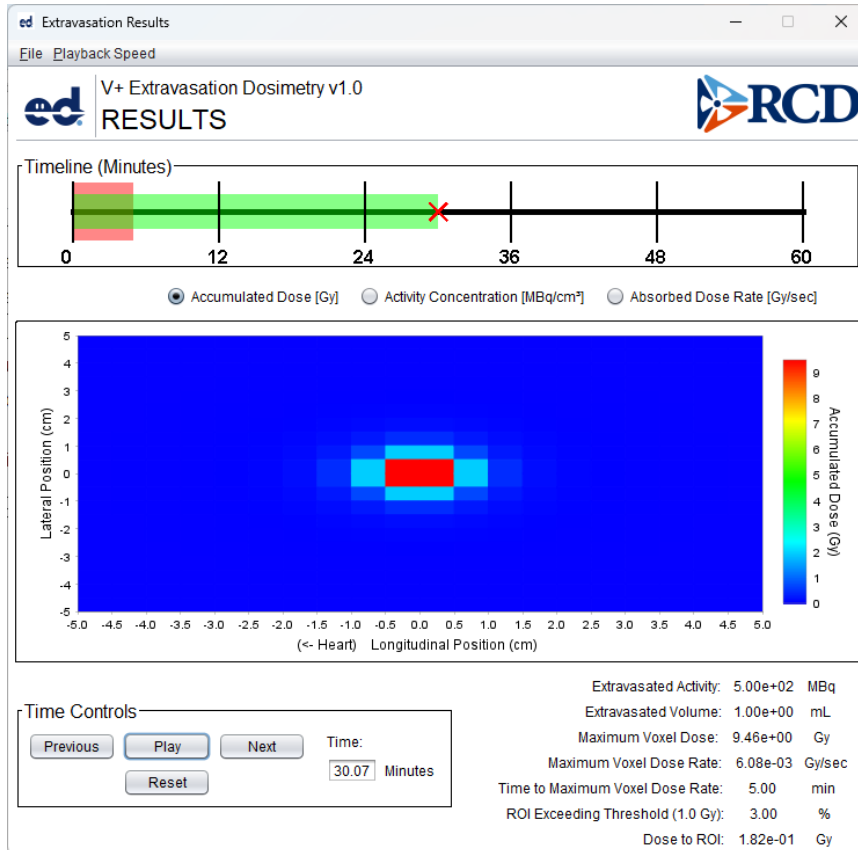


Figure 4-2 Results screen showing the subject seven outputs in the bottom panel.

The reported Maximum Voxel Dose (9.46 Gy) is an accumulated value at the end of the analysis period. This calculation is equal to the maximum voxel dose appearing in Figure 4-3 and is confirmed. This value can also be found in a printout of the Extravasation Report.

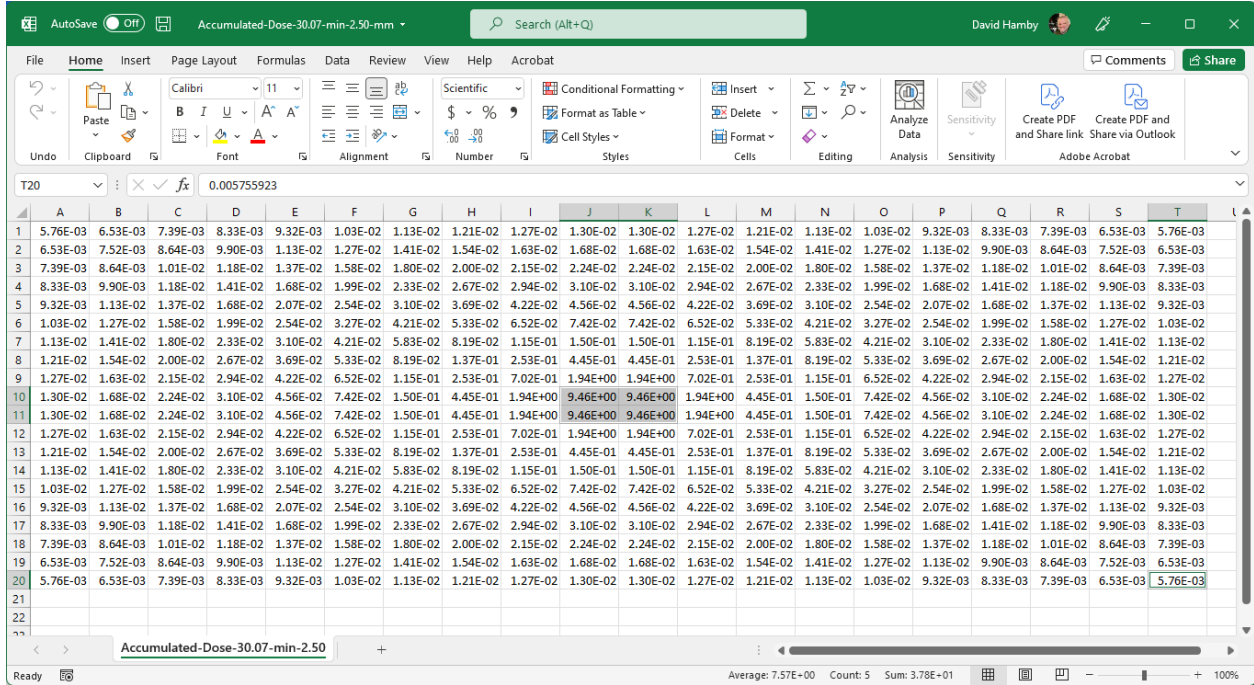


Figure 4-3 Results report (.csv format) for accumulated dose at the end of the analysis.

The Maximum Voxel Dose Rate (6.08 mGy/s) occurring at the 5-minute point of analysis is confirmed (Figure 4-4) by the dose rate report at the final timestep.

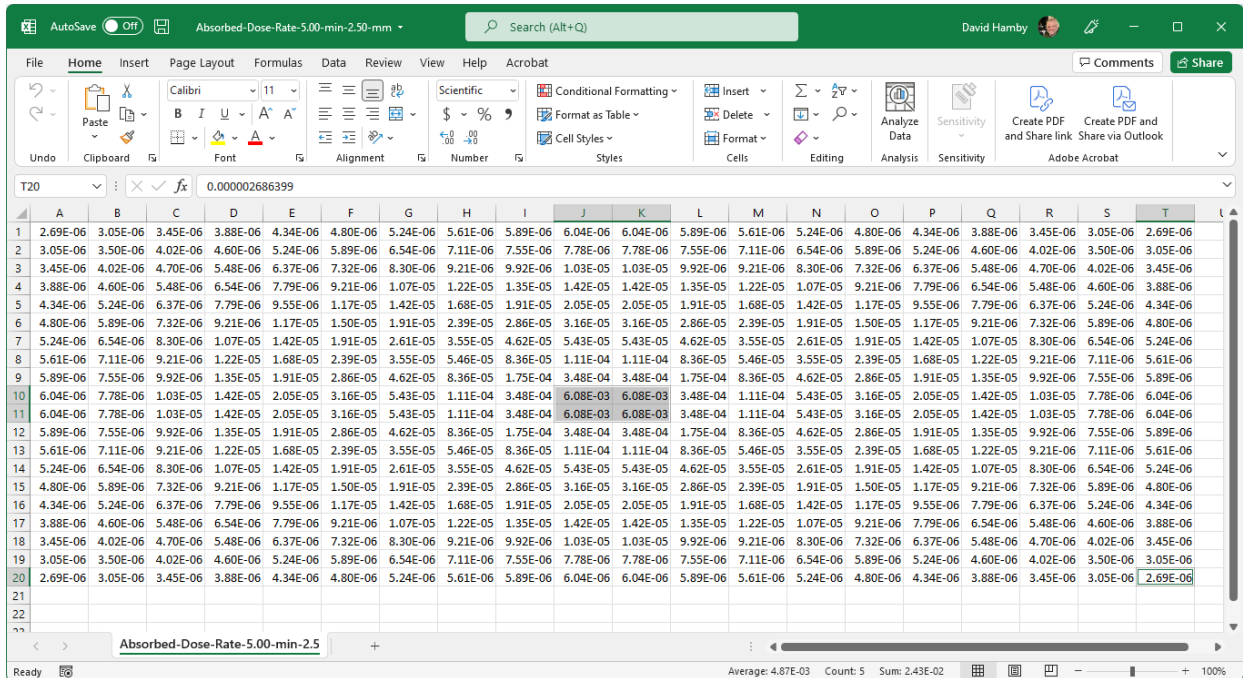


Figure 4-4 Results report (.csv format) for absorbed dose rate in the last timestep of the analysis.

Time to Maximum Voxel Dose is reasonable because the activity is slow to move, its radiological half-life is long, and the dissipation rates are set to very low values. We would only expect that total dose to the region continues to rise during a short analysis time.

Dose to ROI is reported as 0.182 Gy. The average Accumulated Dose to all cells at the end of analysis is 0.182 Gy (Figure 4-5). The Dose to ROI displayed is confirmed.

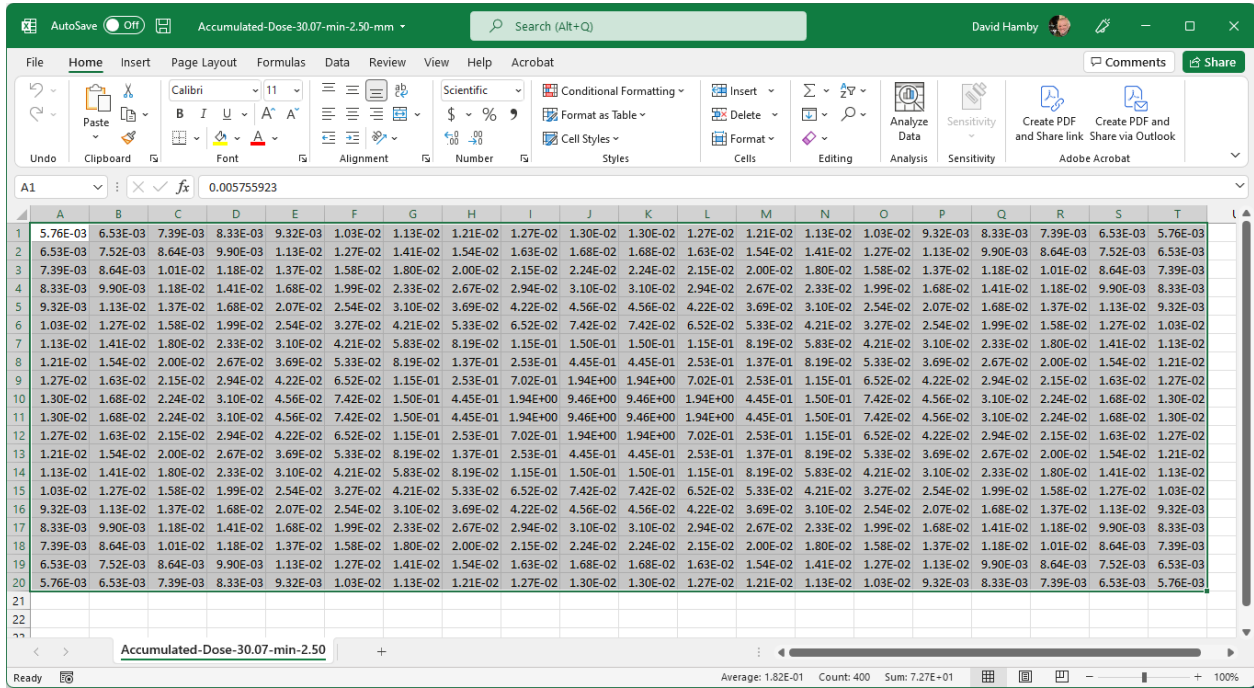


Figure 4-5 Results report for Dose to ROI in the last timestep revealing the average dose over all calculational cells.

The percentage of the ROI exceeding the dose threshold (1 Gy) in this case is reported as 3%. Therefore, of the four-hundred Accumulated Dose values at the end of analysis, twelve of them should be above 1 Gy. That is confirmed (Figure 4-6).

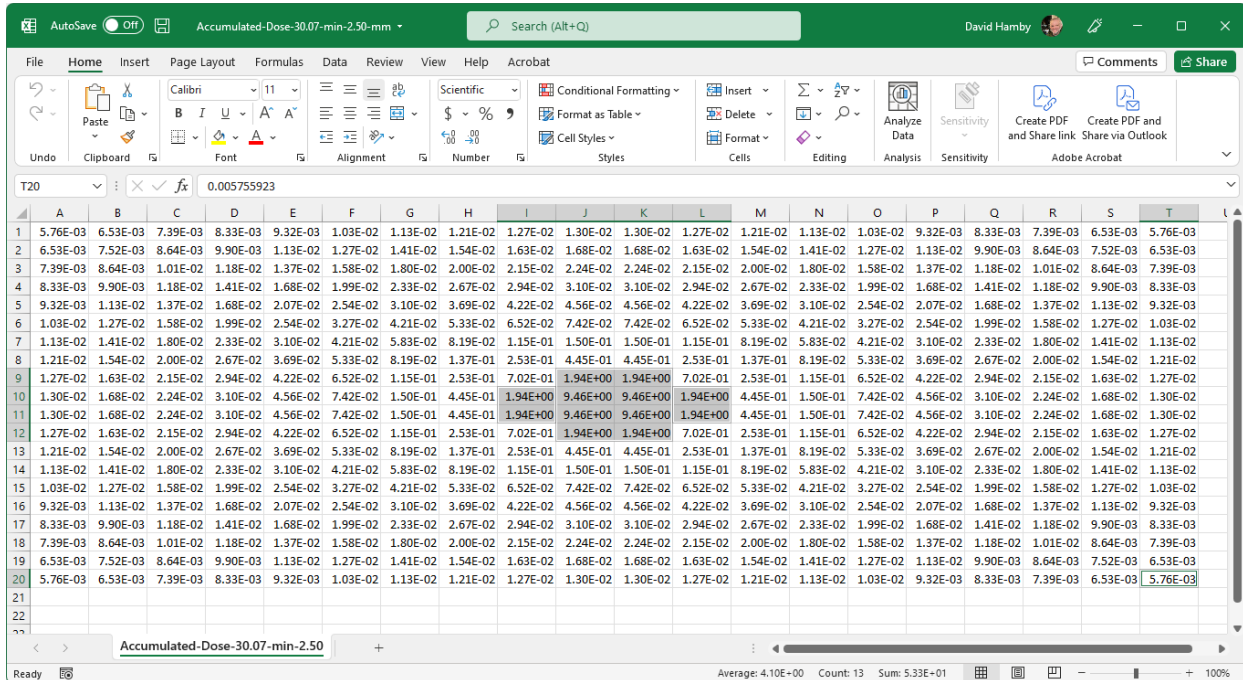


Figure 4-6 Results report for accumulated dose in the last timestep revealing four cells in excess of the 1 Gy dose threshold.

## 4.2. Pure Alpha Decay

Gadolinium (Gd)-148 is a long half-life (70.9 years), pure alpha emitter with a yield of 100%, an alpha energy of 3.18277 MeV (with a range of 0.002 cm in tissue), and a recoil energy of 0.0884678 MeV (ICRP 2008).

To check alpha dosimetry calculations, a “Basic” simulation in ExtravDose was modeled (Figure 4-7) with Gd-148 at a concentration of 100 MBq/mL and a constant flow rate of 1 mL/min.



ed Extravasation Dosimetry v1.0

File Mode Help

ed V+ Extravasation Dosimetry v1.0

MODEL INPUTS

RCD

Source and Concentration Inputs

Database:  ICRP-38  ICRP-107 Concentration: 100.000 MBq/mL

Nuclide: Gd-148 Flow Rate: 1.000 mL/min

Layer Inputs

Tissue Model:  Homogeneous

Number of Layers: 1

Layer 1

Effective Tissue Thickness: 5.000 mm

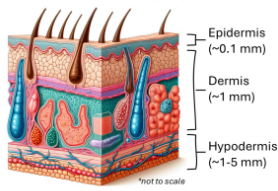
Transport Inputs

Dose Notification Threshold: 2.000 Gy

Region Width: 10.000 cm

Region Length: 20.000 cm

Diagram



Timeline Calculate Results

Figure 4-7 Basic model inputs for a Gd-148 simulation.

Over the course of a 5-minute extravasation event a total of 500 MBq is extravasated at the injection site. The Region of Interest in this event is assumed to be 10 cm wide by 20 cm in length, and 0.5 cm deep (a total volume of 100 cm<sup>3</sup>, with eight-hundred 0.125 cm<sup>3</sup> computational volumes). All basic input variables and the timeline are kept at their default values. The 30-minute simulation requires a clock time of about 25 seconds (Figure 4-8).

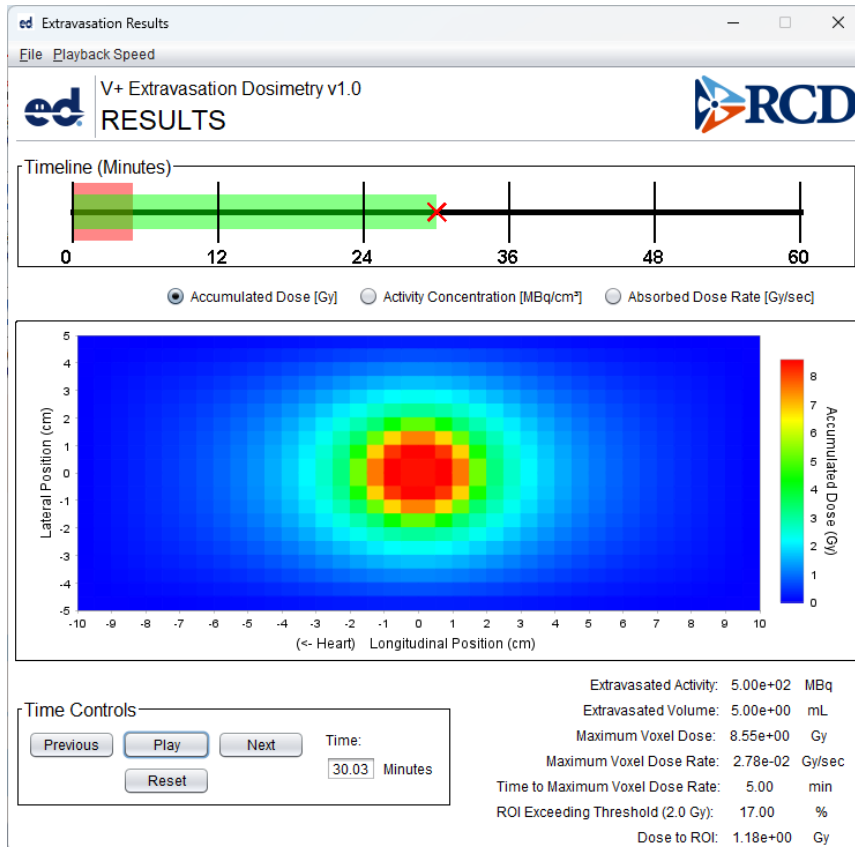


Figure 4-8 Accumulated Dose at the end of analysis for Gd-148.

For confirmation of alpha dose contribution, activity concentration and absorbed dose rate at the first timestep of 0.02 minutes are examined. We see that only the four central cells contain alpha-emitting activity (Figure 4-9).

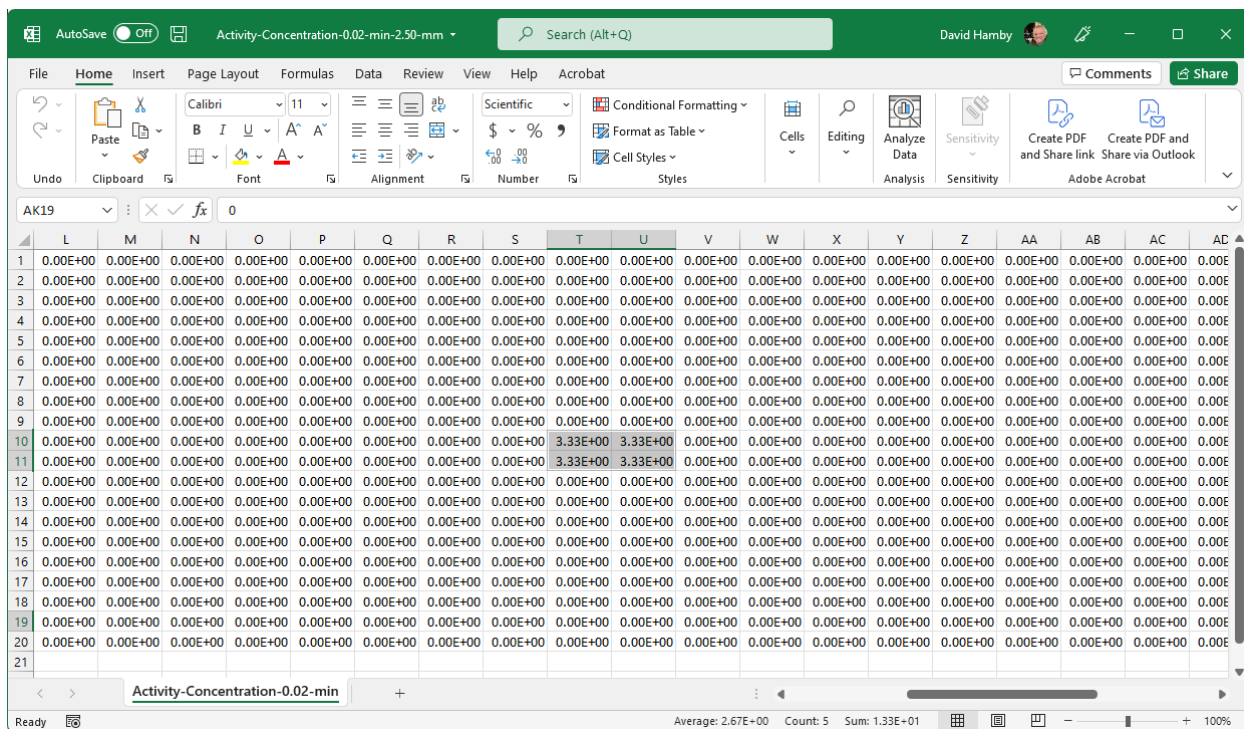


Figure 4-9 Activity concentration at the first timestep.

At that time, the activity concentration in the middle calculational cells is recorded as 3.33 MBq/cm<sup>3</sup>. The absorbed dose rate (Eqn. [2.28]) to the same calculational cell is therefore:

$$\dot{D}_{\alpha S} = 1.602 \times 10^{-10} \frac{3.33 \times 10^6 \cdot 1 \cdot 3.27}{1.1} \left( 1 - 3 \frac{0.002}{0.5} \right) = 1.57 \times 10^{-3} \left[ \frac{\text{Gy}}{\text{s}} \right]$$

and the dose rate contribution to an adjacent cell (Eqn. [2.29]) is:

$$\dot{D}_{\alpha A} = 1.602 \times 10^{-10} \frac{3.33 \times 10^6 \cdot 1 \cdot 3.27}{1.1} \left( \frac{0.002}{2 \cdot 0.5} \right) = 3.17 \times 10^{-6} \left[ \frac{\text{Gy}}{\text{s}} \right]$$

The ed. module reports (Figure 4-10) that the highest voxel dose rate at 0.02 minutes is 1.57x10<sup>-3</sup> Gy/s and the adjacent voxel dose is 3.14x10<sup>-6</sup> Gy/s. The code reports 17% of the ROI voxels exceed the threshold dose (2 Gy) and that is confirmed by Accumulated Dose output at the end of analysis (Figure 4-11).

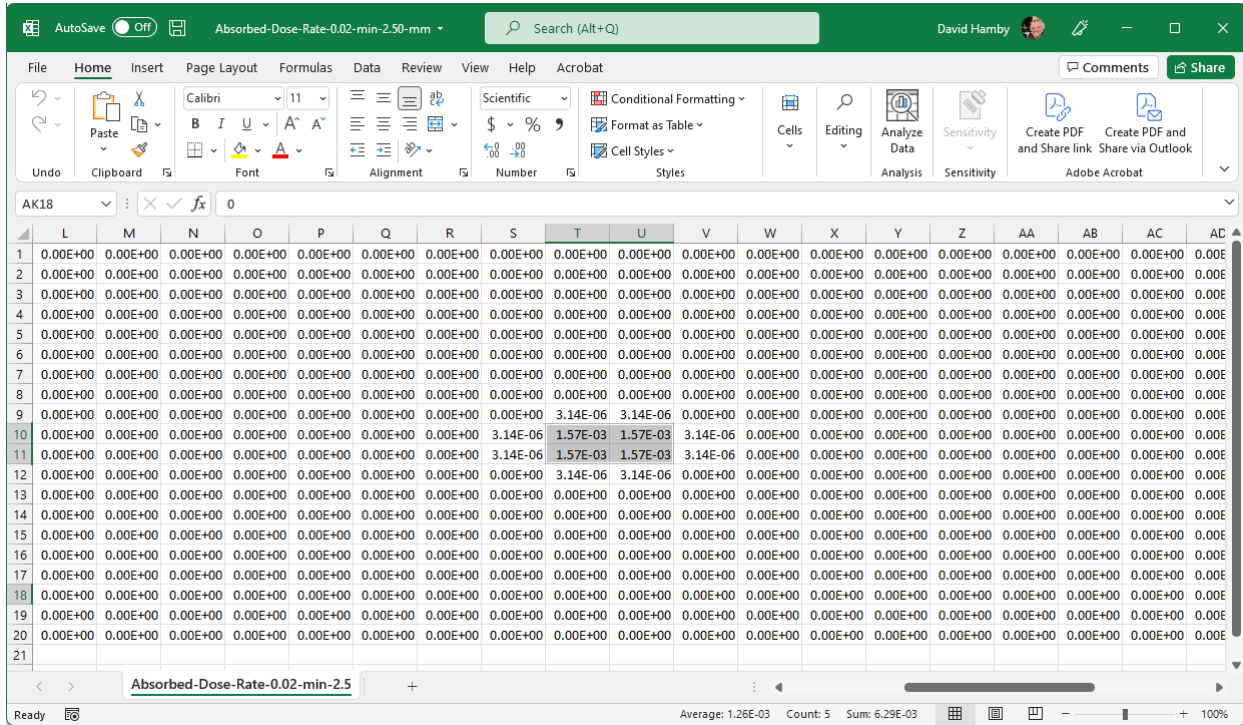


Figure 4-10 Absorbed dose report at the first simulation timestep indicating alpha dose to source cells and to adjacent cells.

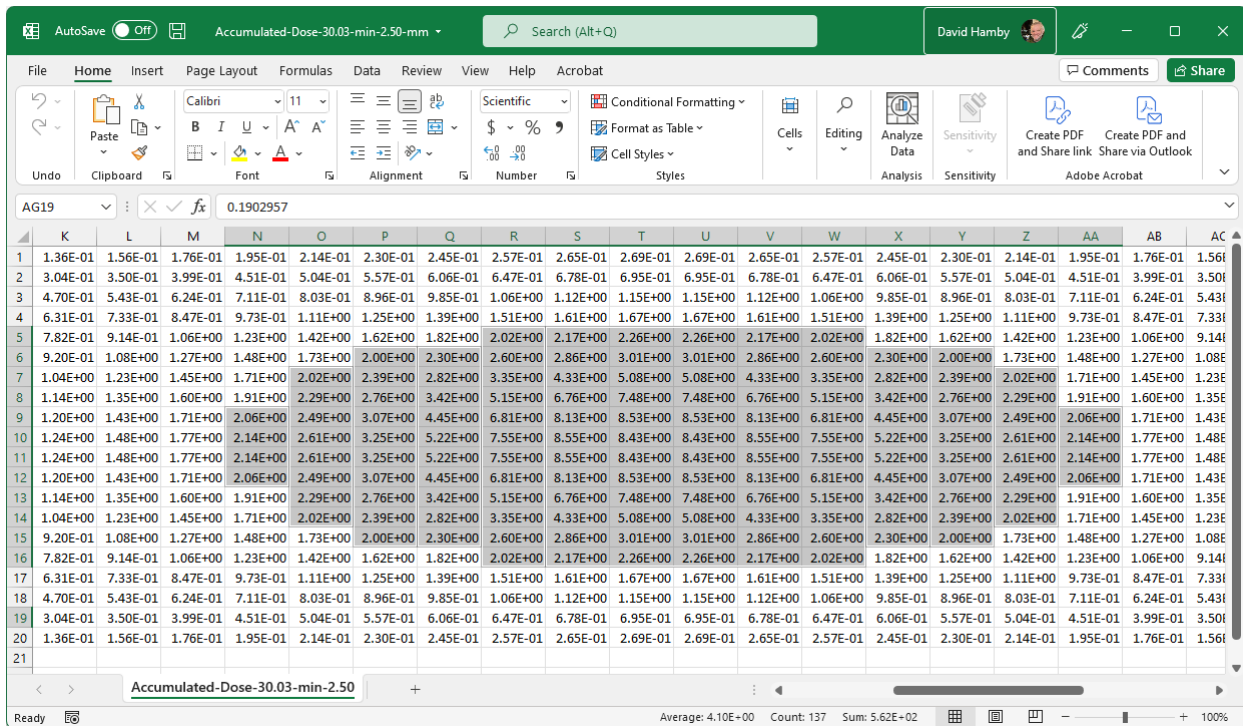


Figure 4-11 Accumulated dose report for the final timestep. 17% of the 800 values (136) are greater than the dose threshold of 2 Gy.

### 4.3. Am-241 Alpha Decay

Americium (Am)-241 is a long half-life (432 years), alpha emitter with a total yield of 99.86%, an average alpha energy of about 5.48 MeV (range = 0.00440 cm), and a recoil energy of about 0.0925 MeV (ICRP 2008). The radionuclide also emits a number of photons and electrons of low yield and low energy, but the energy absorption is insignificant (<10%) compared to the high-energy alpha.

The Advanced calculation in ed. was modeled as an Am-241 concentration of 1 mCi/mL in a flow rate of 1 mL/min over a 5-minute period for a total of 5 mL and 185 MBq extravasated at the injection site (Figure 4-12). The extravasate region of interest is assumed to be homogeneous and 10 cm wide by 10 cm in length, with an effective tissue thickness of 1 cm and lateral transmissivity of 0.3 cm<sup>2</sup>/h. The voxel side length is 1 cm. This simulation results in 100 calculational cells all with a volume of 1 cm<sup>3</sup>. A dose notification threshold of 10 Gy was employed with vertical transmissivity and fluid diffusivity kept at their default values (1.0 and 0.1 cm<sup>2</sup>/h, respectively). The evaluation requires a clock time of about 13 seconds to run a 60-minute simulation.

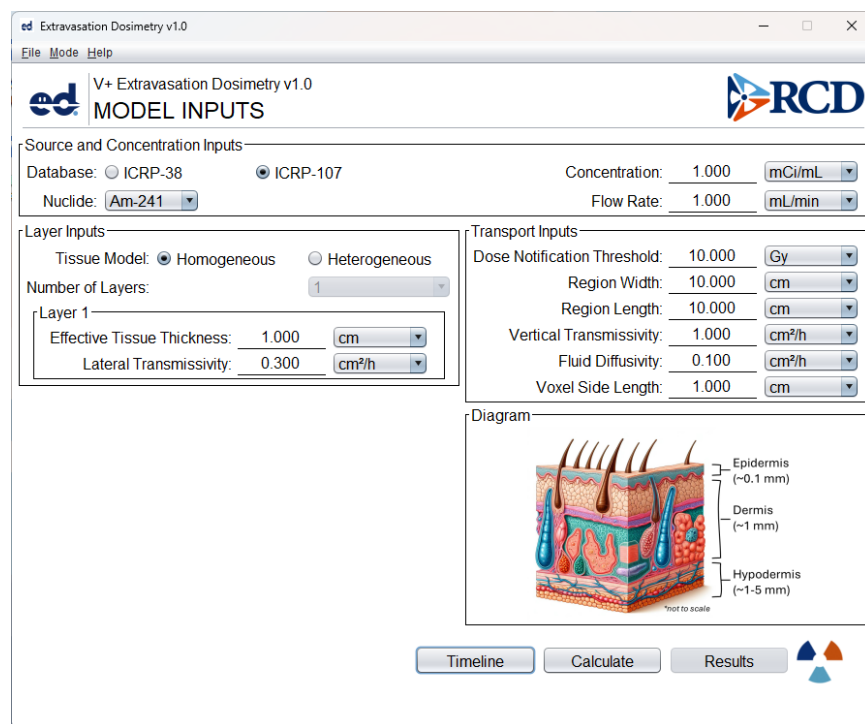


Figure 4-12 Simulation input for Am-241 problem.

The output data (Figure 4-14) indicate that 12% of the region of interest exceeds the dose threshold, the maximum voxel dose is 20.7 Gy, and the absorbed Dose to ROI is 3.86 Gy. The analysis indicates that the maximum voxel dose rate occurs at 5 minutes after the beginning of extravasation. At that timestep, the highest activity concentration is

recorded as  $14.2 \text{ MBq/cm}^3$  (Figure 4-13). The absorbed dose rate to the same calculational cell is therefore:

$$\dot{D}_{\alpha S} = 1.602 \times 10^{-10} \frac{1.42 \times 10^7 \cdot 1 \cdot 5.57}{1.1} \left( 1 - 3 \frac{0.0044}{1.0} \right) = 0.0114 \left[ \frac{\text{Gy}}{\text{s}} \right]$$

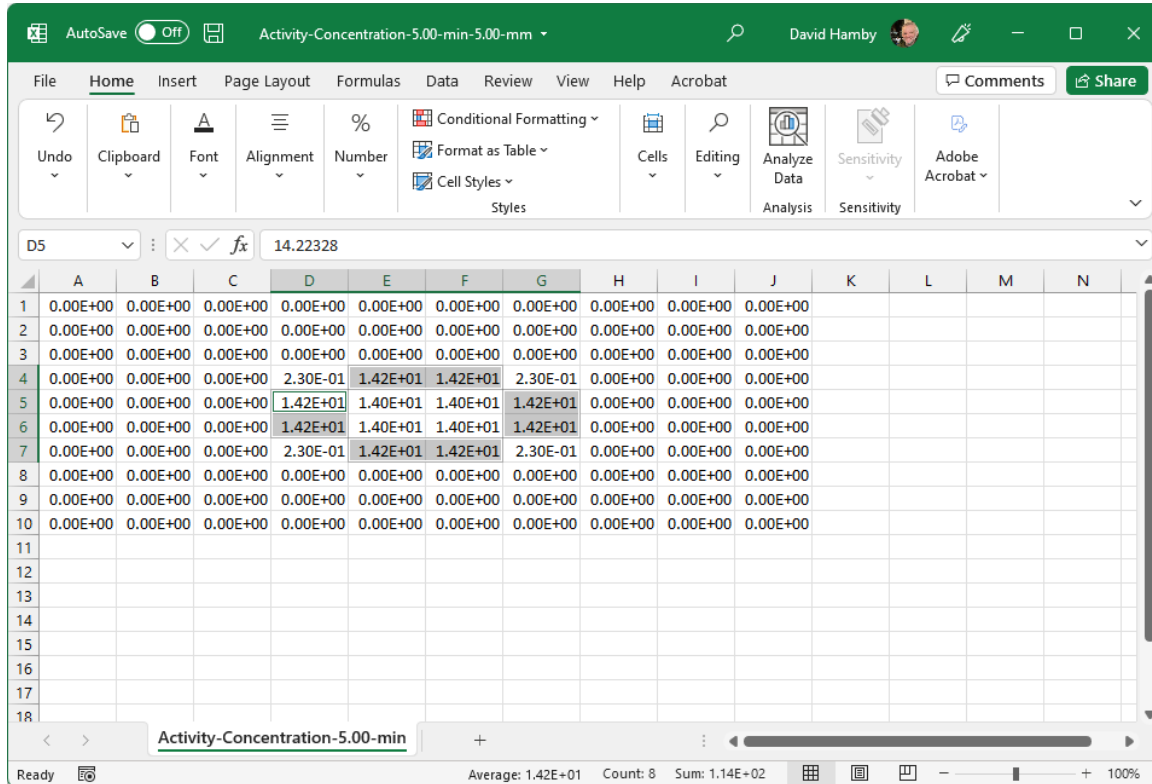


Figure 4-13 Simulation output for Am-241 problem.

The ExtravDose simulation compares with the self-irradiated dose rate of 0.0115 Gy/s in the computational cell. The calculation is confirmed (Figure 4-14).

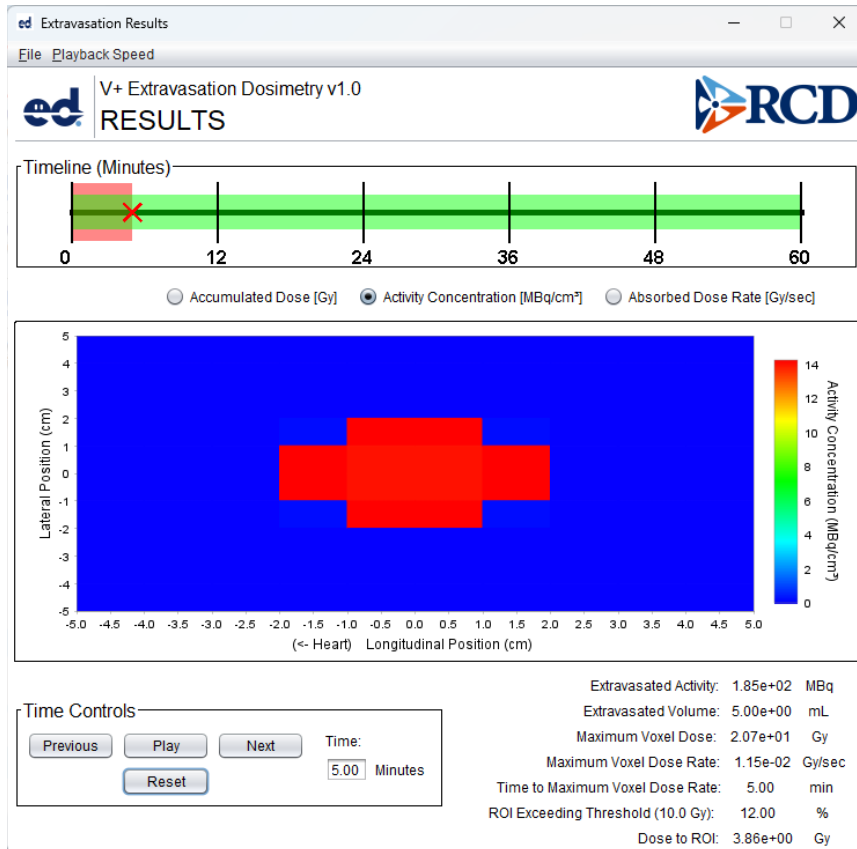


Figure 4-14 Simulation output for Am-241 problem.

#### 4.4. Co-60 Photons

Cobalt (Co)-60 is a beta emitter (5.27-y half-life) with two prominent, high-energy photons. The electrons have an average energy of about 96 keV with an  $X_{90}$  of 0.033 cm. Its two photons are 1.173 and 1.332 MeV (average of 1.25 MeV), both emitted 100% of decays. The  $\mu_{en}/\rho$  of the average photon energy is 0.0293 cm<sup>2</sup>/g and the average  $\mu$  is 0.0626 cm<sup>-1</sup>.

The result window is shown in Figure 4-16. In the first time-step of the analysis (0.02 minutes), the activity concentration in the center of the ROI is equal to 3.33 MBq/cm<sup>3</sup> (Figure 4-17). There are 800 cells (0.125 cm<sup>3</sup> each) and only the middle four contain Co-60 (0.416 MBq per computational cell).



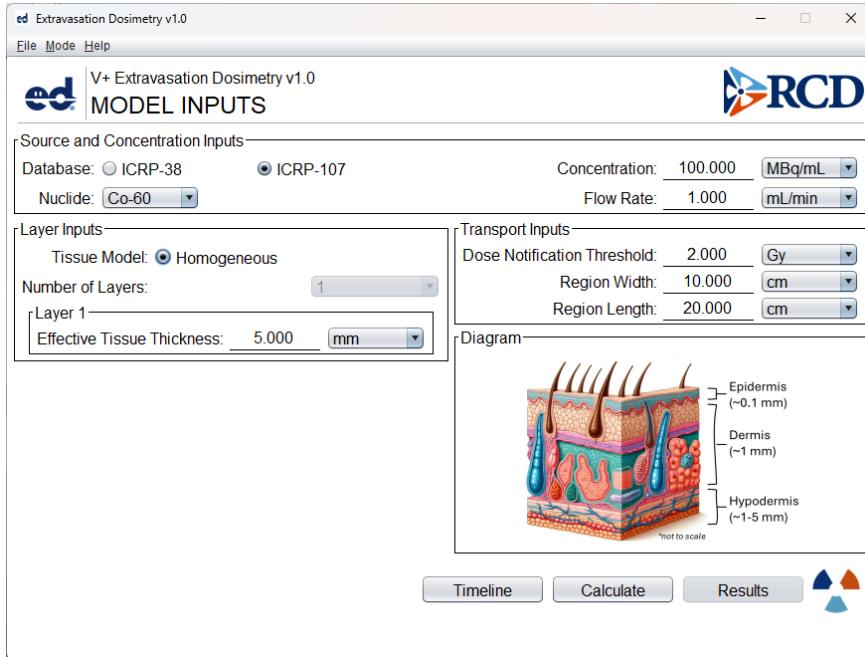


Figure 4-15 Basic inputs for a Co-60 simulation.

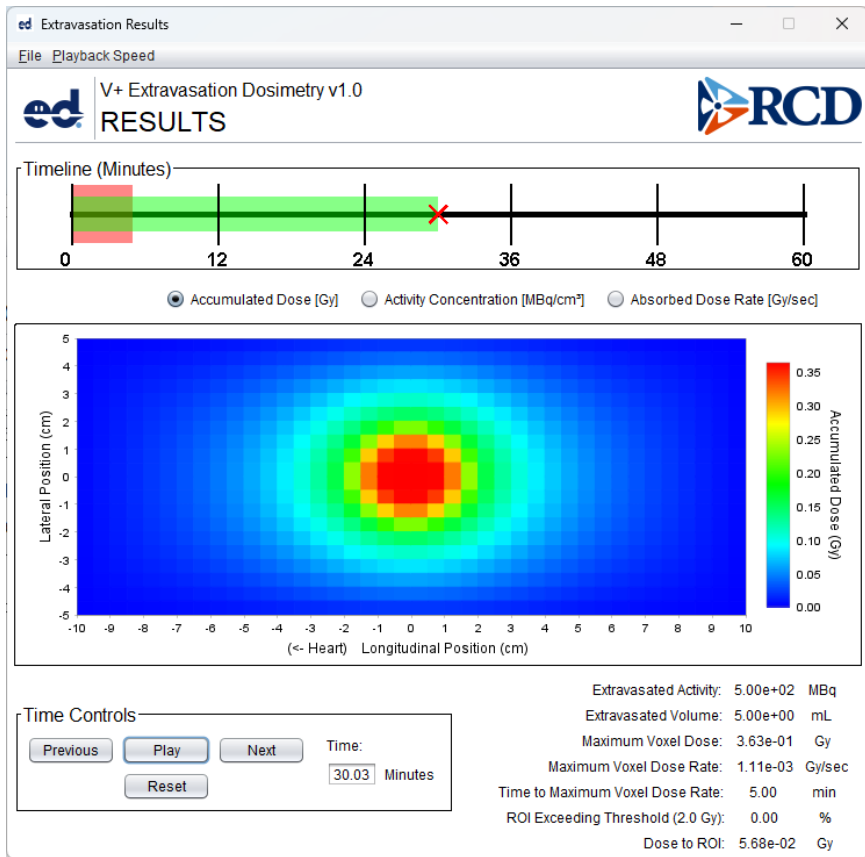


Figure 4-16 Results for a Co-60 simulation showing accumulated dose.



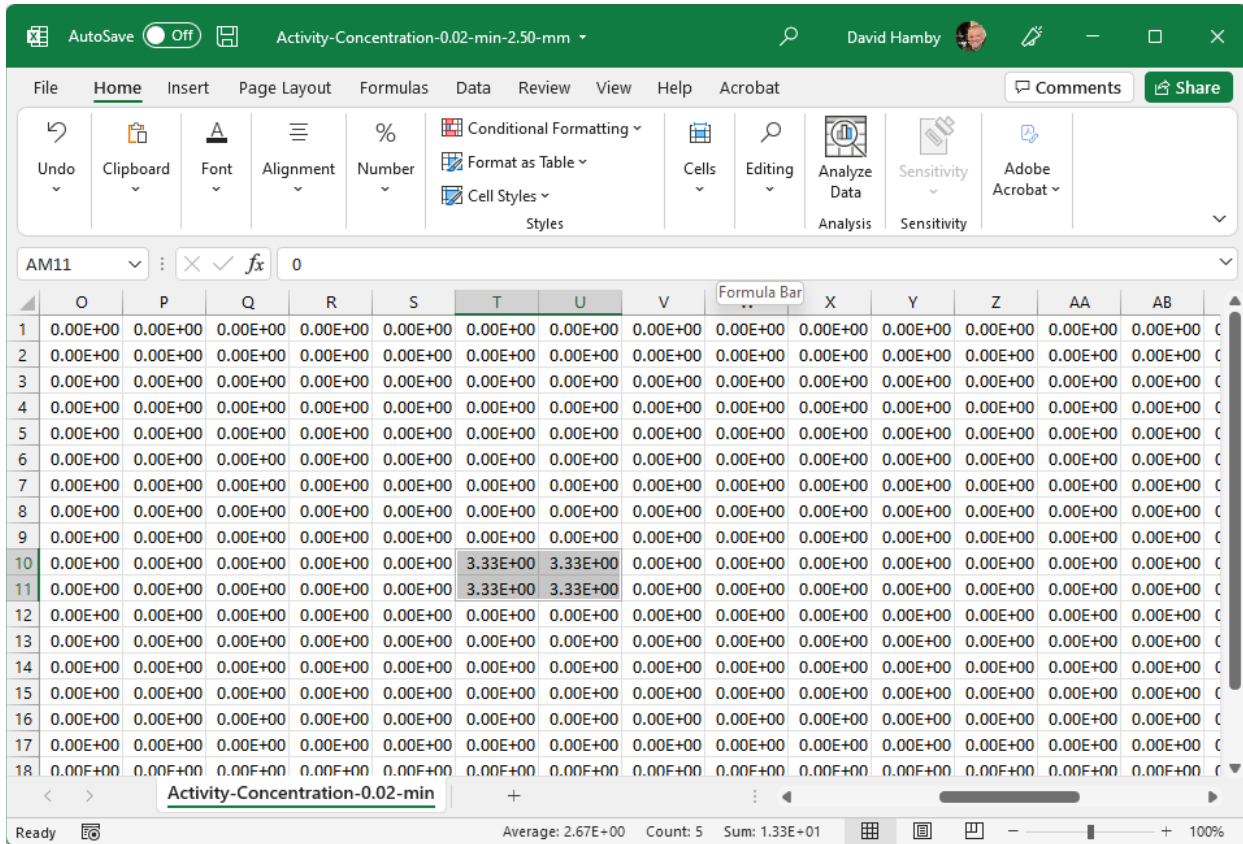


Figure 4-17 Showing the four central source cells with activity at the first time step.

The dose confirmation calculation is conducted for a target cell that is 4 and 4.5 cm from the central source cells (see Figure 4-18). The dose rate result at 0.2 minutes reveals a positive dose rate in every calculation cell with a value of  $6.90 \times 10^{-8}$  Gy/s in the target cell (L10). This dose is due solely to the Co-60 photon emissions.

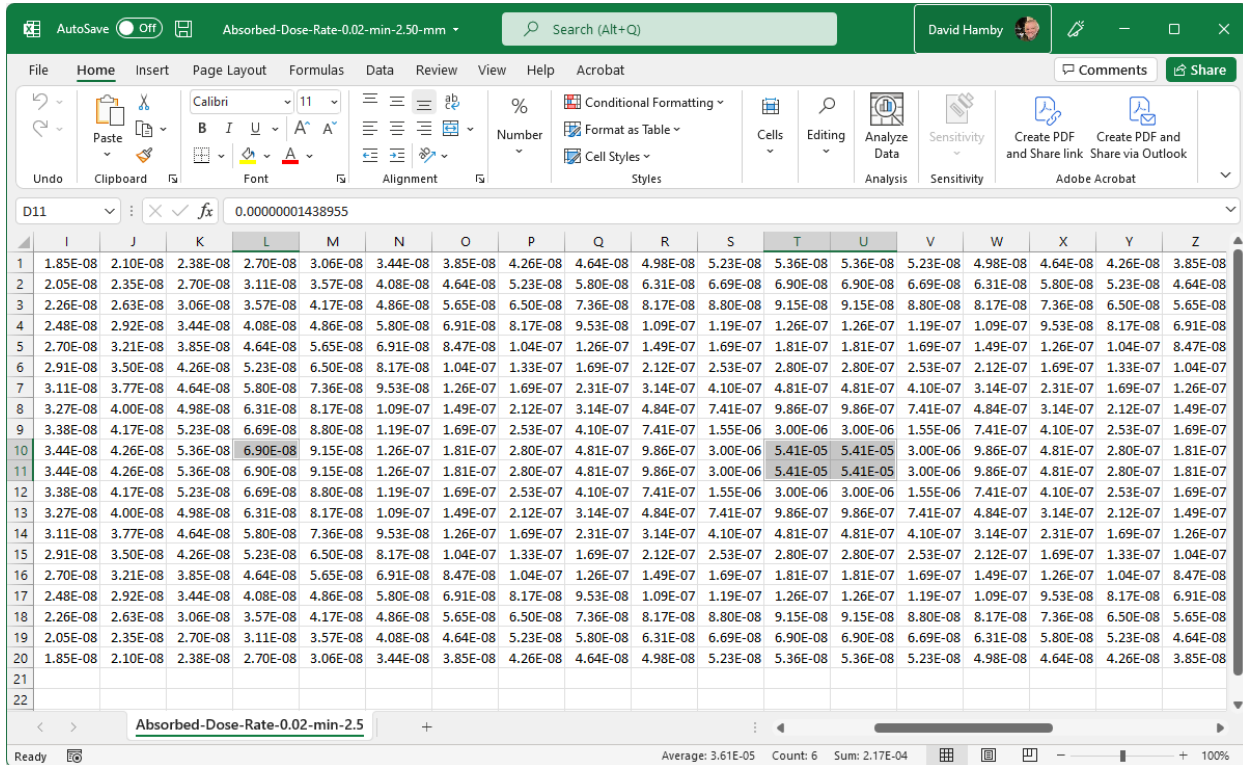


Figure 4-18 Results reported for absorbed dose rate in calculational cells at 0.02 minutes after extravasation. The source (right) and target (left) cells are highlighted.

The photon dose rate in cell L10 is due to activity in each of the four center voxels. That dose rate is calculated to be:

$$\dot{D}_\gamma = \frac{1.602 \times 10^{-10} \left[ \frac{Jg}{MeV kg} \right] \cdot 2 \cdot 4.16 \times 10^5 \left[ \frac{nt}{s} \right] \cdot 1.25 \left[ \frac{MeV}{\gamma} \right] \cdot 2 \left[ \frac{\gamma}{nt} \right] \cdot 0.0293 \left[ \frac{cm^2}{g} \right] \cdot e^{-0.0626 \cdot 4}}{4\pi \cdot 4^2 [cm^2]}$$

$$\dot{D}_\gamma = 3.78 \times 10^{-8} \left[ \frac{Gy}{s} \right]$$

from the two cells at 4 cm, and

$$\dot{D}_\gamma = \frac{1.602 \times 10^{-10} \left[ \frac{Jg}{MeV kg} \right] \cdot 2 \cdot 4.16 \times 10^5 \left[ \frac{nt}{s} \right] \cdot 1.25 \left[ \frac{MeV}{\gamma} \right] \cdot 2 \left[ \frac{\gamma}{nt} \right] \cdot 0.0293 \left[ \frac{cm^2}{g} \right] \cdot e^{-0.0626 \cdot 4.5}}{4\pi \cdot 4.5^2 [cm^2]}$$

$$\dot{D}_\gamma = 2.89 \times 10^{-8} \left[ \frac{Gy}{s} \right]$$

from the two cells at 4.5 cm. The sum of those doses is  $6.67 \times 10^{-8}$  Gy/s in the target cell, a difference of about 3% from the ExtravDose calculated value. ExtravDose will execute

the dosimetry calculation for each individual photon and with more precision, therefore this difference is quite acceptable.

#### 4.5. Pure Beta Decay

Yttrium (Y)-90 is a pure beta emitter (64-hour half-life) in that only beta particles (negatively charged electrons) are emitted. These electrons possess an energy above zero to 2.28 MeV, with an average energy of 0.934767 MeV and a 100% yield. The  $X_{90}$  is 0.538 cm.

The Advanced calculation in ed. was modeled as 1 mL of extravasated fluid (using a 1 mL/min flow rate for 1 minute) with a Y-90 concentration of 250 MBq/mL for a total of 100 MBq extravasated at the injection site. Calculational cells are 0.5 cm cubed ( $0.125 \text{ cm}^3$ ), the region width and length are 10 cm, and the effective tissue thickness is 0.5 cm, and the lateral transmissivity is set to  $0.1 \text{ cm}^2/\text{h}$ . All other variables are kept with the default value and the analysis period is 30 minutes in total (Figure 4-19). This analysis results in 400 cubes that create a region of interest that is 10 cm long x 10 cm wide x 0.5 cm deep ( $50 \text{ cm}^3$ ). The 30-minute simulation requires a clock time of about 10 seconds to run (Figure 4-20).

The screenshot shows the 'Extravasation Dosimetry v1.0' software interface. The window title is 'V+ Extravasation Dosimetry v1.0' and the main heading is 'MODEL INPUTS'. The interface is divided into several sections:

- Source and Concentration Inputs:**
  - Database:  ICRP-38  ICRP-107
  - Nuclide:
  - Concentration: 250.000 MBq/mL
  - Flow Rate: 1.000 mL/min
- Layer Inputs:**
  - Tissue Model:  Homogeneous  Heterogeneous
  - Number of Layers: 1
  - Layer 1:
    - Effective Tissue Thickness: 5.000 mm
    - Lateral Transmissivity: 0.100  $\text{cm}^2/\text{h}$
- Transport Inputs:**
  - Dose Notification Threshold: 2.000 Gy
  - Region Width: 10.000 cm
  - Region Length: 10.000 cm
  - Vertical Transmissivity: 1.000  $\text{cm}^2/\text{h}$
  - Fluid Diffusivity: 0.100  $\text{cm}^2/\text{h}$
  - Voxel Side Length: 5.000 mm
- Diagram:** A cross-sectional diagram of skin layers with labels:
  - Epidermis (~0.1 mm)
  - Dermis (~1 mm)
  - Hypodermis (~1-5 mm)

At the bottom of the window, there are buttons for 'Timeline', 'Calculate', and 'Results', along with a small logo.

Figure 4-19 Input window for Y-90 example.

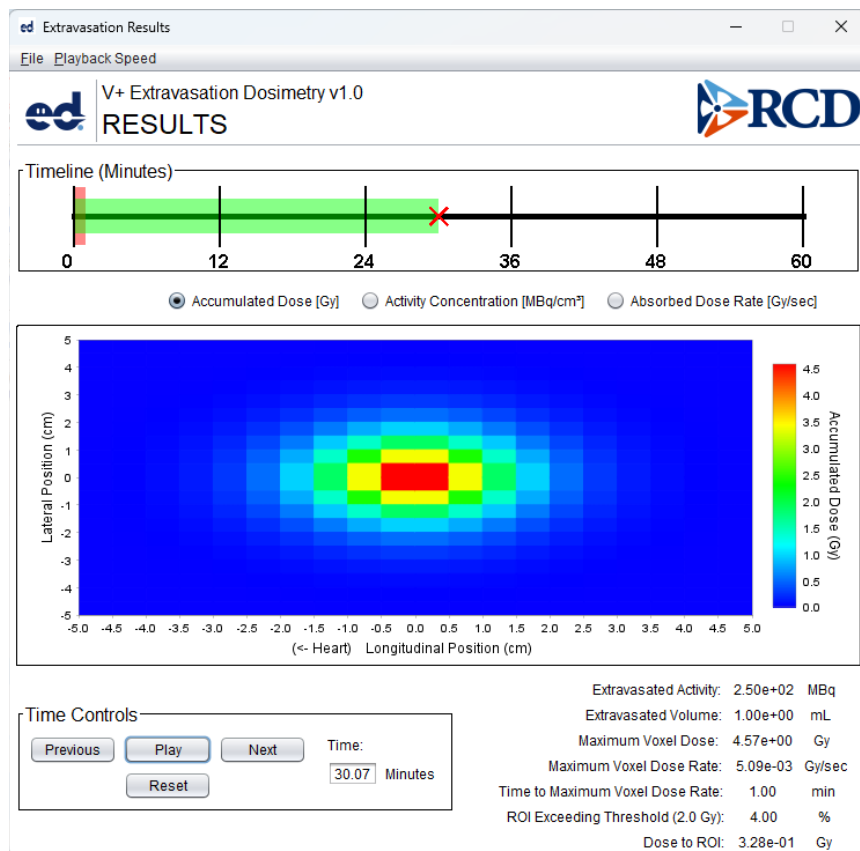


Figure 4-20 Results report for accumulated dose over all calculational cells.

To confirm near electron calculations, the four central calculation cells in the first timestep (Figure 4-21) has a positive concentration of  $8.33 \text{ MBq/cm}^3$  in  $0.125 \text{ cm}^3$  (containing  $1.04 \times 10^6 \text{ Bq}$ ). The target cell is the same as the source cell, and  $X_{90}$  is equal to  $0.538 \text{ cm}$ , so that  $r = \sqrt[2]{3} s = 0.333 \text{ cm}$ . Equation [2.31] is used below to calculate the electron dose rate at those distances. The source self-irradiating results in an  $F_e(\xi, E_0)$  of  $0.878$ .

$$\dot{D}_e(0.333) = \frac{(1.6 \times 10^{-10})(1.04 \times 10^6)(1)(0.935)(0.878)}{(1.1)(4\pi)(0.333)^2(0.538)} = 1.66 \times 10^{-4} \left[ \frac{\text{Gy}}{\text{s}} \right]$$

$$\dot{D}_e(0.5) = \frac{(1.6 \times 10^{-10})(2)(1.04 \times 10^6)(1)(0.935)(0.580)}{(1.1)(4\pi)(0.5)^2(0.538)} = 9.71 \times 10^{-5} \left[ \frac{\text{Gy}}{\text{s}} \right]$$

$$\dot{D}_e(0.707) = \frac{(1.6 \times 10^{-10})(1.04 \times 10^6)(1)(0.935)(0.244)}{(1.1)(4\pi)(0.707)^2(0.538)} = 1.02 \times 10^{-5} \left[ \frac{\text{Gy}}{\text{s}} \right]$$

A simple sum the contributions calculated above is  $2.73 \times 10^{-4} \text{ Gy/s}$ . The dose rate predicted to the source cell in this simulation from all sources is  $2.39 \times 10^{-4} \text{ Gy/s}$  (Figure 4-22), a difference of about 12%. Again, this is acceptable since the hand calculation is a simplification of the many additional calculations occurring in ExtravDose.

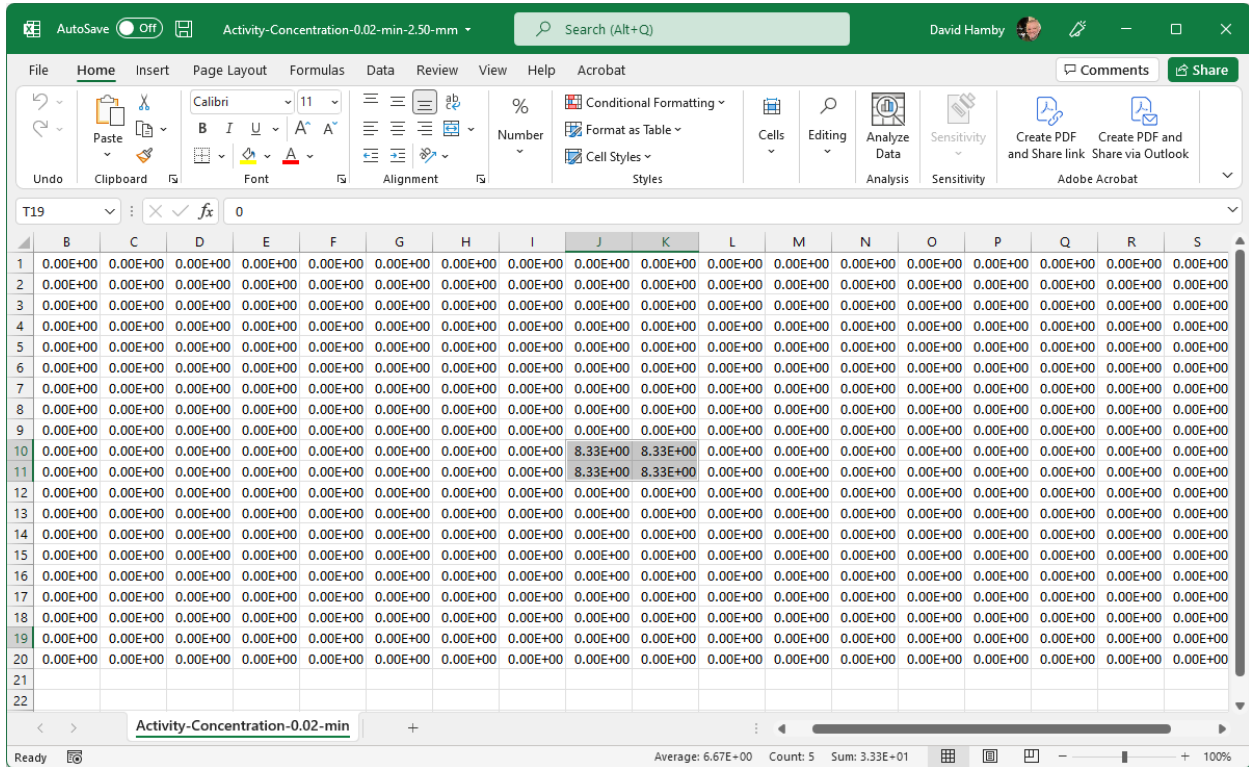


Figure 4-21 Activity concentration in the calculational cells at the first timestep.

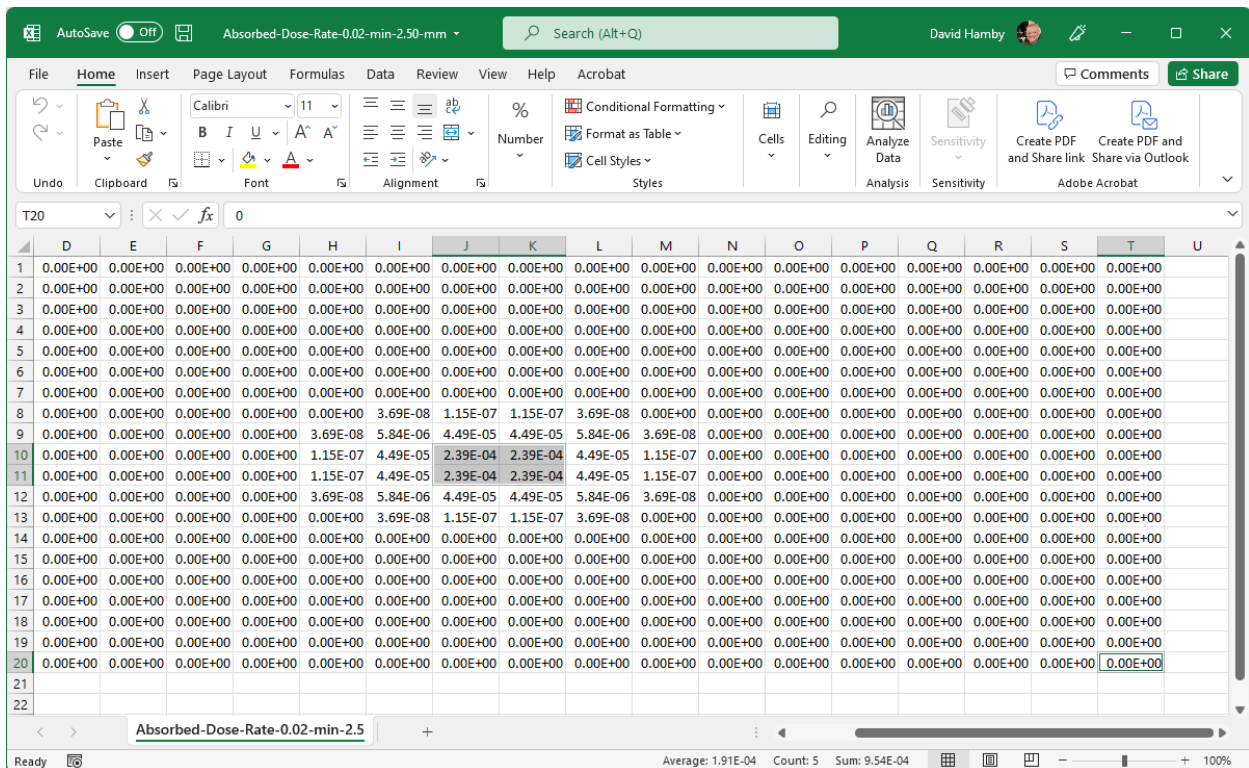


Figure 4-22 Absorbed dose rate in the calculational cells at the first timestep.

To confirm distant electron calculations, as in the last example, central calculational cells have a positive concentration of 8.33 MBq/cm<sup>3</sup> in 0.125 cm<sup>3</sup> (containing 1.04x10<sup>6</sup> Bq in each of the four central cells) and no other cells are populated with radioactivity.

One target cell (cell K9 in Figure 4-22) is chosen that is 0.5 cm from one source cell (cell K10), 0.707 cm from another source cell (cell J10), 1.0 cm from another (cell K11), and 1.12 cm from the last (cell J11). Equation [2.30] is used below to calculate the electron dose rate at each of those distances to contribute to dose in cell K9. The  $F_e(\xi)$  for each distance is 0.580, 0.244, 0.0227, and 0.0150, respectively. Therefore, the dose calculation goes as such:

$$\dot{D}_e(0.5) = \frac{(1.6 \times 10^{-10})(1.04 \times 10^6)(1)(0.935)(0.580)}{(1.1)(4\pi)(0.5)^2(0.538)} = 4.85 \times 10^{-5} \left[ \frac{\text{Gy}}{\text{s}} \right]$$

and likewise,

$$\dot{D}_e(0.707) = \frac{(1.6 \times 10^{-10})(1.04 \times 10^6)(1)(0.935)(0.244)}{(1.1)(4\pi)(0.707)^2(0.538)} = 1.02 \times 10^{-5} \left[ \frac{\text{Gy}}{\text{s}} \right]$$

$$\dot{D}_e(1.0) = \frac{(1.6 \times 10^{-10})(1.04 \times 10^6)(1)(0.935)(0.0227)}{(1.1)(4\pi)(1.0)^2(0.538)} = 4.75 \times 10^{-7} \left[ \frac{\text{Gy}}{\text{s}} \right]$$

$$\dot{D}_e(1.12) = \frac{(1.6 \times 10^{-10})(1.04 \times 10^6)(1)(0.935)(0.0150)}{(1.1)(4\pi)(1.12)^2(0.538)} = 2.50 \times 10^{-7} \left[ \frac{\text{Gy}}{\text{s}} \right]$$

The sum of the dose rates above ( $5.94 \times 10^{-5}$  Gy/s) is compared to  $4.49 \times 10^{-5}$  Gy/s in cell K9 (Figure 4-23), a difference of about 24% from the dose rate calculated by the extravasation dosimetry module.



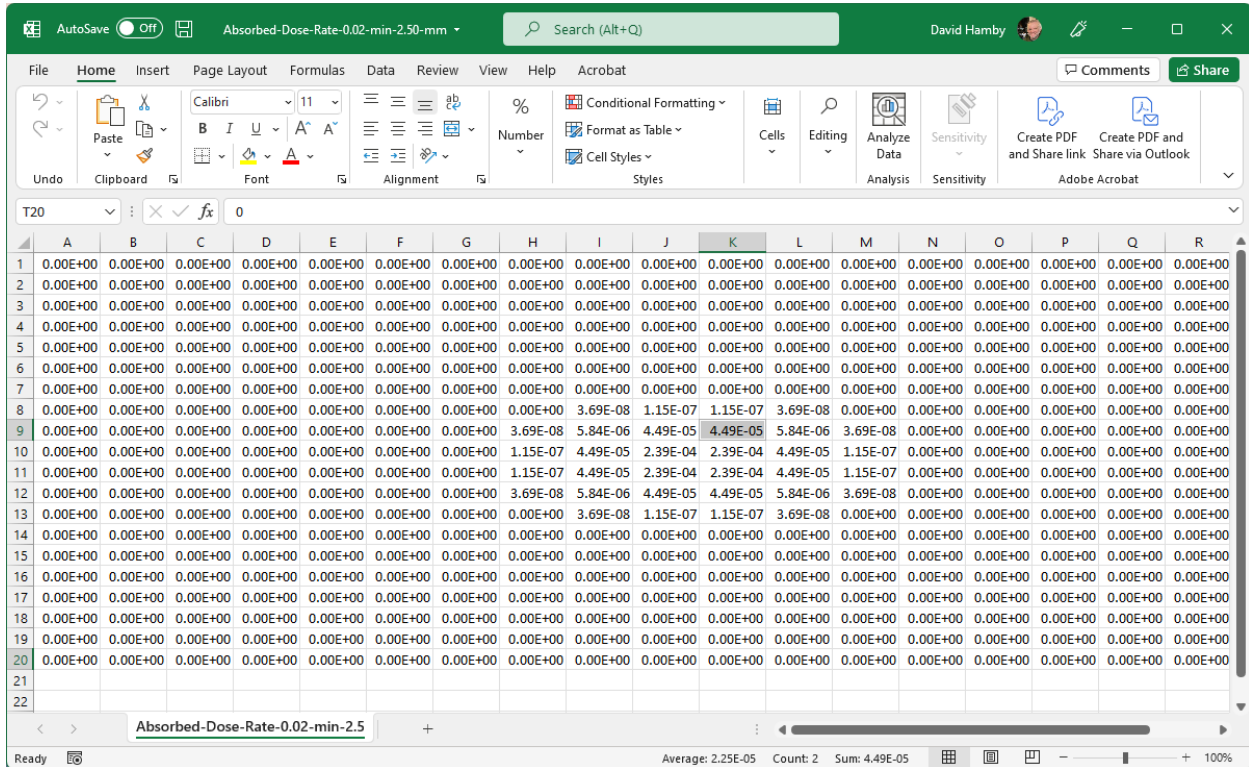
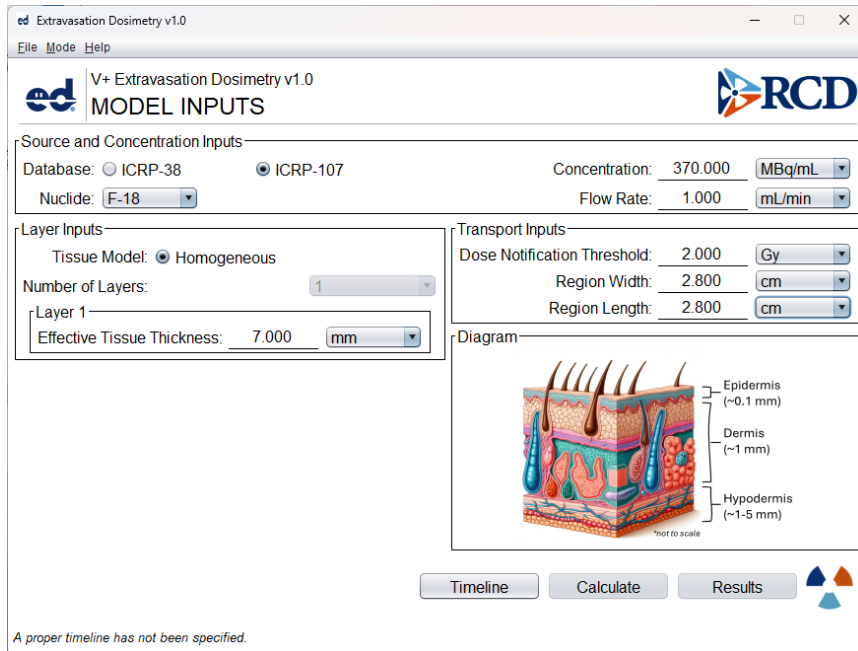


Figure 4-23 Absorbed dose rate in the first time step from activity in the four central cells.

#### 4.6. F-18 Comparison to Extravasation Calculation in the Literature

Fluorine-18 (ICRP 107) is used for positron emission tomography (PET) imaging with a typical administered activity of 10 mCi (370 MBq), as described by Tiwari et al. (2024). Tiwari et al. (2024) assumed a uniform distribution of <sup>18</sup>F activity within a “5.5-mL” volume in the hypodermis with dimensions of 0.7 cm thick, 2.8 cm wide, and 2.8 cm long. Figure 4-24 and Figure 4-25 show V+ inputs for the same total activity and tissue dimensions with an analysis time of 4 h, which is slightly longer than two radiological half-lives. Because the V+ extravasation module includes removal processes not explicitly modeled by Tiwari et al. (2024), the V+ calculation proceeded with the total administered activity, which may be considered as advantageous for not requiring users to apply *a priori* assumptions or obtain *a posteriori* estimates to specify another input parameter for the fraction of administered activity involved in the extravasation.



ed Extravasation Dosimetry v1.0

File Mode Help

V+ Extravasation Dosimetry v1.0  
MODEL INPUTS

Source and Concentration Inputs

Database:  ICRP-38  ICRP-107 Concentration: 370.000 MBq/mL

Nuclide: F-18 Flow Rate: 1.000 mL/min

Layer Inputs

Tissue Model:  Homogeneous

Number of Layers: 1

Layer 1

Effective Tissue Thickness: 7.000 mm

Transport Inputs

Dose Notification Threshold: 2.000 Gy

Region Width: 2.800 cm

Region Length: 2.800 cm

Diagram

Epidermis (~0.1 mm)

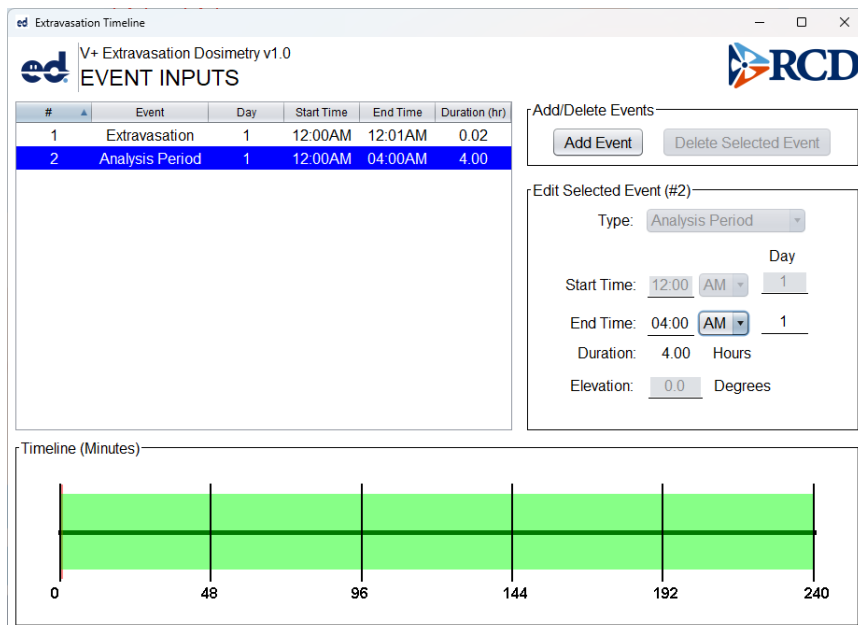
Dermis (~1 mm)

Hypodermis (~1-5 mm)

Timeline Calculate Results

A proper timeline has not been specified.

Figure 4-24 Input parameters for a basic calculation with  $^{18}\text{F}$ .



ed Extravasation Timeline

V+ Extravasation Dosimetry v1.0  
EVENT INPUTS

#	Event	Day	Start Time	End Time	Duration (hr)
1	Extravasation	1	12:00AM	12:01AM	0.02
2	Analysis Period	1	12:00AM	04:00AM	4.00

Add/Delete Events

Add Event Delete Selected Event

Edit Selected Event (#2)

Type: Analysis Period

Day

Start Time: 12:00 AM 1

End Time: 04:00 AM 1

Duration: 4.00 Hours

Elevation: 0.0 Degrees

Timeline (Minutes)

0 48 96 144 192 240

Figure 4-25 Timeline inputs for a basic calculation with  $^{18}\text{F}$ .

The V+ simulation finished in about 25 seconds. Figure 4-26 is the extravasation dose report showing a dose to the ROI of 150 mGy with a maximum voxel dose of 358 mGy. To determine the impact of additional V+ removal processes (i.e., vascular-lymphatic removal of radioactive fluid from the tissue ROI and radioactive fluid flow outside the small tissue ROI) on calculated doses, V+ activity concentrations within the tissue ROI were



manually extracted at various time steps and compared to expected activities from radioactive decay alone. Because time-integrated reductions in activity by ExtravDose were a factor of 10 greater than those modeled by Tiwari et al. (2024), V+ results were multiplied by 10 for comparison. In other words, V+ would return an average dose of about 1.5 Gy to the tissue ROI and maximum voxel dose of about 3.6 Gy if loss mechanisms other than radioactive decay were removed for the 4-h analysis for the same amount of extravasated radioactivity. These V+ results are generally consistent with the 1.32-Gy dose published by Tiwari et al. (2024) for radioactivity restricted to and uniformly distributed within a  $\sim 5.5\text{-cm}^3$  hypodermis ROI.

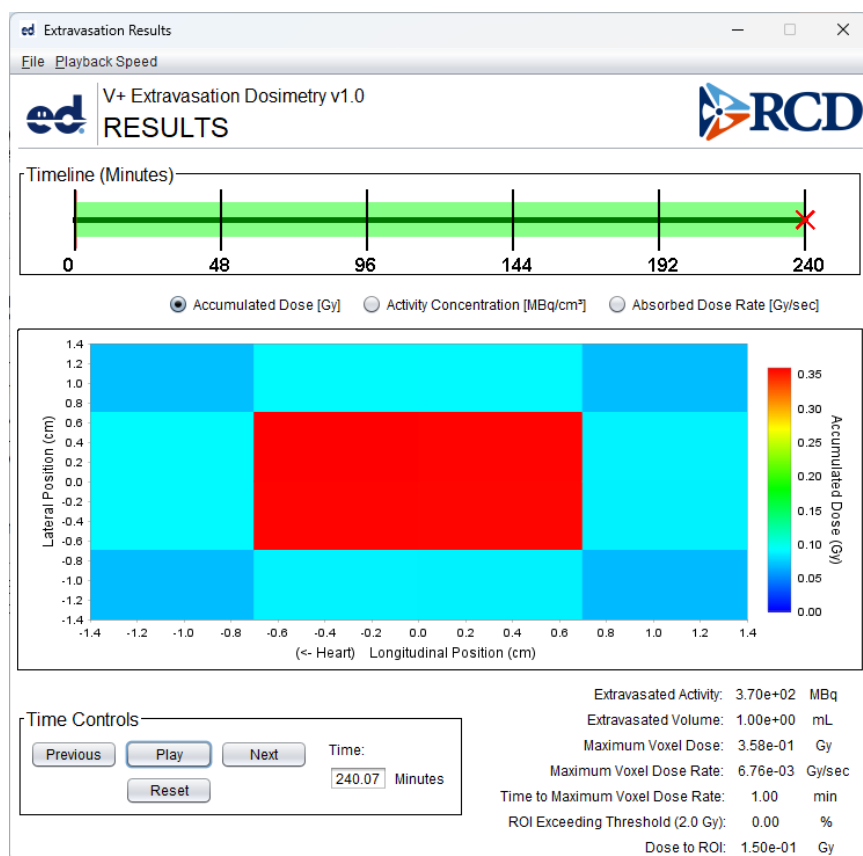


Figure 4-26 Dose results for  $^{18}\text{F}$  extravasation in local tissue.

## 5.0 REFERENCES

- Aijaz, M.; Almanjahie, I.M.; Dar, I.G. Mathematical estimation of fluid concentration in human skin during water immersion. *Journal of Advanced Research*. 28: 1-6. 2021.
- Aquino-Guerrero, M. Tackling extravasation. *British Journal of Nursing*. 31(19): S3. 2022.
- Arveschoug, A.K.; Bekker, A.C.; Iversen, P.; Bluhme, H.; Villadsen, G.E.; Staantum, P.F. Extravasation of [<sup>177</sup>Lu]Lu-dotatoc: case report and discussion. *European Journal of Nuclear Medicine and Molecular Imaging Research (EJNMMI Research)* 10:68. 7 pages. 2020.
- Aukland, K.; Reed, R.K. Interstitial-lymphatic mechanisms in the control of extracellular fluid volume. *Physiological Reviews*. 73(1): 1-78. 1993.
- Benke, R.R.; Bartlow, N.E.; Luitjens, J.M.; Hamby, D.M. Radiopharmaceutical Extravasation Modeling of Local Tissue Dose. Renaissance Code Development, LLC. Report No. RCD-23-212-2. Corvallis, OR: 2023.
- Berry, K.; Kendrick, J. Lutetium-177 radiopharmaceutical therapy extravasation lessons learned. *Health Phys* 123(2): 160-164. 2022.
- Bonta, D.V.; Halkar, R.K.; Alazraki, N. Extravasation of a therapeutic dose of <sup>131</sup>I-metaiodobenzylguanidine: prevention, dosimetry, and mitigation. *J Nucl Med* 52(9): 1418-1422. 2011.
- Breen, S.L.; Driedger, A.A. Radiation injury from interstitial injection of Iodine-131-iodocholesterol. Letters to the Editor. *J Nucl Med* 32(5): 892. 1991.
- Castronovo, F.P., Jr.; McKusick, K.A.; Strauss, H.W. The infiltrated radiopharmaceutical injection: dosimetric considerations. *Eur J Nucl Med* 14: 93-97. 1988.
- Centers for Disease Control and Prevention (CDC). Cutaneous Radiation Injury: A Brochure for Physicians. <https://www.cdc.gov/nceh/radiation/emergencies/crphysicianfactsheet.htm> (website accessed on September 18, 2023). 2023.
- Grodzinsky, A.J. Fields, Forces, and Flows in Biological Systems. Garland Science. 2011.
- Guyton, A.C.; Scheel, K.; Murphree, D. Interstitial fluid pressure. III. Its effect on resistance to tissue fluid mobility. *Circ. Res.* 19: 412-419. 1966.

Hamby, D.M.; Luitjens, J.M.; Tucker, Z.G.; Mangini, C.; Rose, C.T.; Flora, R.S. V+ Technical Manual Series: Skin Dosimetry Module. U.S. Nuclear Regulatory Commission. RIL 2025-06. Renaissance Code Development RCD-24-324-0. December 2024.

International Atomic Energy Agency (IAEA). Medical Management of Radiation Injuries. Safety Reports Series No. 101. Vienna, Austria. 2020.

International Commission on Radiation Protection (ICRP). Radiation and Your Patient: A Guide for Medical Practitioners. ICRP Supporting Guidance 2. Ann. ICRP 31(4). 2001.

International Commission on Radiological Protection (ICRP). The 2007 Recommendations of the International Commission on Radiological Protection. ICRP Publication 103. Ann. ICRP 37(2-4). 2007.

International Commission on Radiological Protection (ICRP). "Nuclear Decay Data for Dosimetric Calculations." Publication 107. Ann. ICRP 38 (3). 2008.

International Commission on Radiological Protection (ICRP). ICRP Statement on Tissue Reactions / Early and Late Effects of Radiation in Normal Tissues and Organs – Threshold Doses for Tissue Reactions in a Radiation Protection Context. ICRP Publication 118. Ann. ICRP 41(1/2). 2012.

International Commission on Radiological Protection (ICRP). Diagnostic Reference Levels in Medical Imaging. ICRP Publication 135. Ann. ICRP 46(1). 2017.

International Commission on Radiological Protection (ICRP). Radiological Protection in Therapy with Radiopharmaceuticals. ICRP Publication 140. Ann. ICRP 48(1). 2019.

International Commission on Radiation Units and Measurements (ICRU). "Tissue Substitutes in Radiation Dosimetry and Measurement." ICRU Report 44. Bethesda, MD: International Commission on Radiation Units and Measurements. 1989.

Iori, M.; Grassi, E.; Lorenzo, P.; Meglioli, G.; Botti, A.; Sceni, G.; Cucurachi, N.; Verzellesi, L.; Finocchiaro, D.; Versari, A.; Fraboni, B.; Fioroni, F. Safety injections of nuclear medicine radiotracers: towards a new modality for a real-time detection of extravasation events and 18F-FDG SUV data correction. *EJNMMI Physics* 10(1), Article 31, 22 pages. 2023.

Kawabe, J.; Higashiyama, S.; Kotani, K.; Yoshida, A.; Tsushima, H.; Yamanaga, T.; Tsuruta, D.; Shiomi, S. Subcutaneous extravasation of Sr-89: Usefulness of Bremsstrahlung imaging in confirming Sr-89 extravasation and in the decision making for the choice of treatment strategies for local radiation injuries caused by Sr-89 extravasation. *Asia Oceania J Nucl Med Biol* 1(2): 56-59. 2013.

Masoodi, R.; Ghanbari, R.N.. Derivation of the Theis (1935) equation by substitution. *Ground water*. 50(1): 8-9. 2012.

Maucherat, B.; Varmenot, N.; Fleury, V.; Senellart, H.; Rousseau, C. Effective management of  $^{177}\text{Lu}$ -DOTA0-Tyr3-Octreotate Extravasation. *Clin Nucl Med* 46(2): 114-145. 2021.

Mazzara, C.; Salvadori, J.; Ritzenthaler, F.; Martin, S.; Porot, C.; Imperiale, A.  $^{177}\text{Lu}$ -DOTA-0-Tyr3-octreotate infusion modeling for real-time detection and characterization of extravasation during PRRT. *EJNMMI Physics* 9:33. 16 pages. 2022.

Minsky, B.D.; Siddon, R.L.; Recht, A.; Nagel, J.S. Dosimetry of aqueous  $^{32}\text{P}$  after soft-tissue infiltration following attempted intravenous administration. *Health Phys* 52(1): 87-89. 1987.

National Council on Radiation Protection and Measurements (NCRP). Radiation Dose Management for Fluoroscopically Guided Interventional Medical Procedures. NCRP Report 168. Bethesda, MD. 2010.

Osborne, D.; Kiser, J.W.; Knowland, J.; Townsend, D.; Fisher, D.R. Patient-specific extravasation dosimetry using uptake probe measurements. *Health Phys* 120(3): 339-343. 2021a.

Osborne, D.; Lattanze, R.; Knowland, J.; Bryant, T.E.; Barvi, I.; Fu, Y.; Kiser, J.W. The scientific and clinical case for reviewing diagnostic radiopharmaceutical extravasation long-standing assumptions. *Front Med* 8:684157. 2021b.

Piechowski, J. and Y. Chaptinel. Evaluation of local dose for a contaminated wound. *Radioprotection*. 39(3):355-366; 2004 (in French).

Shapiro, B.; Pillay, M.; Cox, P.H. Dosimetric consequences of interstitial extravasation following IV administration of a radiopharmaceutical. *Eur J Nucl Med* 12: 522-523. 1987.

Shultis, J.K. and Faw, R.E. Radiation Shielding. American Nuclear Society. ISBN 0-89448-4567. La Grange Park, IL. 2000.

Tiwari, A.; Andriotty, M.; Agasthya, G.; Sunderland, J.J.; Osborne, D.R.; Kapadia, A.J. Dosimetric and biological impact of activity extravasation of radiopharmaceuticals in PET imaging. *Med Phys* 52: 801-813. 2024.

Tsorxe, I.Y.; Hayes, R.B. Dose estimation for extravasation of  $^{177}\text{Lu}$ ,  $^{99\text{m}}\text{Tc}$ , and  $^{18}\text{F}$ . *Health Phys* 124(3): 217-220. 2023.

Tsorxe, I.Y.; Hayes, R.B. Dose estimation for extravasation of  $^{177}\text{Lu}$ ,  $^{99\text{m}}\text{Tc}$ , and  $^{18}\text{F}$ . Online report. North Carolina State University: Raleigh, NC. February 2021.

Tylski, P.; Pina-Jomir, G.; Bournaud-Salinas, C.; Jalade, P. Tissue dose estimation after extravasation of  $^{177}\text{Lu}$ -dotatate. *EJNMMI Physics* 8:33. 15 pages. 2021.

U.S. Department of Health and Human Services (HHS). Radiation Emergency Medical Management. <https://remm.hhs.gov> (website last updated on January 19, 2023). 2023.

Williams, G.; Palmer, M.R.; Parker, J.A.; Joyce, R. Extravasation of therapeutic Yttrium-90-ibritumomab tiuxetan (Zevalin<sup>®</sup>): a case report. *Cancer Biother Radiopharm* 21(2): 101-105. 2006.

Wilson, S.; Osborne, D.; Long, M.; Knowland, J.; Fisher, D.R. Practical tools for patient-specific characterization and dosimetry of radiopharmaceutical extravasation. *Health Phys* 123(5): 343-347. 2022.